ACS POLYMERS Au
AN OPEN ACCESS JOURNAL OF THE AMERICAN CHEMICAL SOCIETY

pubs.acs.org/polymerau

Perspective

# Strategies for the Development of Conjugated Polymer Molecular Dynamics Force Fields Validated with Neutron and X-ray Scattering

Caitlyn M. Wolf,* Lorenzo Guio, Sage Scheiwiller, Viktoria Pakhnyuk, Christine Luscombe, and Lilo D. Pozzo*

Cite This: *ACS Polym. Au* 2021, 1, 134–152

Read Online

ACCESS | Metrics & More | Article Recommendations | Supporting Information

**ABSTRACT:** Conjugated polymers (CPs) enable a wide range of lightweight, lower cost, and flexible organic electronic devices, but a thorough understanding of relationships between molecular structure and dynamics and electronic performance is critical for improved device efficiencies and for new technologies. Molecular dynamics (MD) simulations offer *in silico* insight into this relationship, but their accuracy relies on the approach used to develop the model's parameters or force field (FF). In this Perspective, we first review current FFs for CPs and find that most of the models implement an arduous reparameterization of inter-ring torsion potentials and partial charges of classical FFs. However, there are few FFs outside of simple CP molecules, e.g., polythiophenes, that have been developed over the last two decades. There is also limited reparameterization of other parameters, such as nonbonded Lennard-Jones interactions, which we find to be directly influenced by conjugation in these materials. We further provide a discussion on experimental validation of MD FFs, with emphasis on neutron and X-ray scattering. We define multiple ways in which various scattering methods can be directly compared to results of MD simulations, providing a powerful experimental validation metric of local structure and dynamics at relevant length and time scales to charge transport mechanisms in CPs. Finally, we offer a perspective on the use of neutron scattering with machine learning to enable high-throughput parametrization of accurate and experimentally validated CP FFs enabled not only by the ongoing advancements in computational chemistry, data science, and high-performance computing but also using oligomers as proxies for longer polymer chains during FF development.

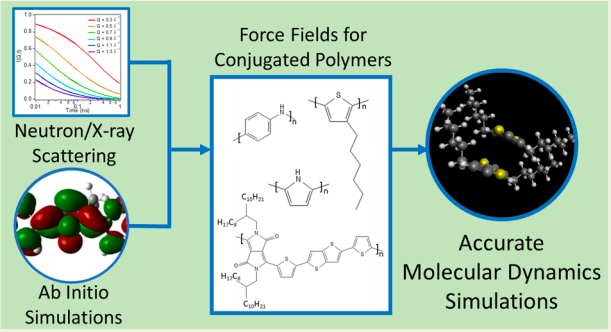


**KEYWORDS:** *conjugated polymers, molecular dynamics simulation, neutron scattering, X-ray scattering, force field, machine learning*

## I. INTRODUCTION

Over the past 50 years, conjugated polymers (CPs) have been applied to a growing number of organic electronic devices. Common examples include organic photovoltaics (OPVs), organic light-emitting diodes (OLEDs), and organic field-effect transistors (OFETs),[1−5] but emerging technologies also include flexible displays, bioelectronics, chemical sensors, and wearable devices.[6−11] CPs provide key advantages by being flexible, lightweight, lower cost, and occasionally biocompatible[12] materials, and a thorough understanding of the relationship between molecular morphology and performance metrics (e.g., electronic conductivity) is necessary to design devices with efficiencies that are competitive with alternatives and that enable wide-scale implementation of new technologies. CPs consist of a $\pi$-conjugated backbone, such as polythiophene, polyacetylene, polyfluorene, or polypyrrole, that enables intrachain charge transport along the chain or interchain charge transport through $\pi$-orbital overlap of neighboring chains.[13] The crystalline phase provides well-ordered chains for extended charge transport through either mechanism. However, charge transport in the amorphous phase can only occur at sporadic $\pi$-orbital overlaps between tie,[14] "looping", or "extending" chains.[13] Therefore, the relationship between structure and dynamics in these phases often determines the limiting rate for charge transport. Finally, flexible side chains are frequently added to the CP structure to increase solubility and to enable solution processing. Researchers have reached the highest efficiencies of organic electronics thus far using donor−acceptor CPs, which consist of alternating donor and acceptor conjugated monomeric units along the backbone.[15,16] Nevertheless, polythiophenes remain the most comprehensively studied CPs, and so, these polymers provide ideal model systems for exploring the structure−function relationship between molecular structure and dynamics, charge transport mechanisms, and macroscopic

Received: August 31, 2021
Revised: October 13, 2021
Accepted: October 14, 2021
Published: November 1, 2021

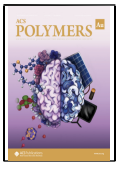





https://doi.org/10.1021/acspolymersau.1c00027
*ACS Polym. Au* 2021, 1, 134–152

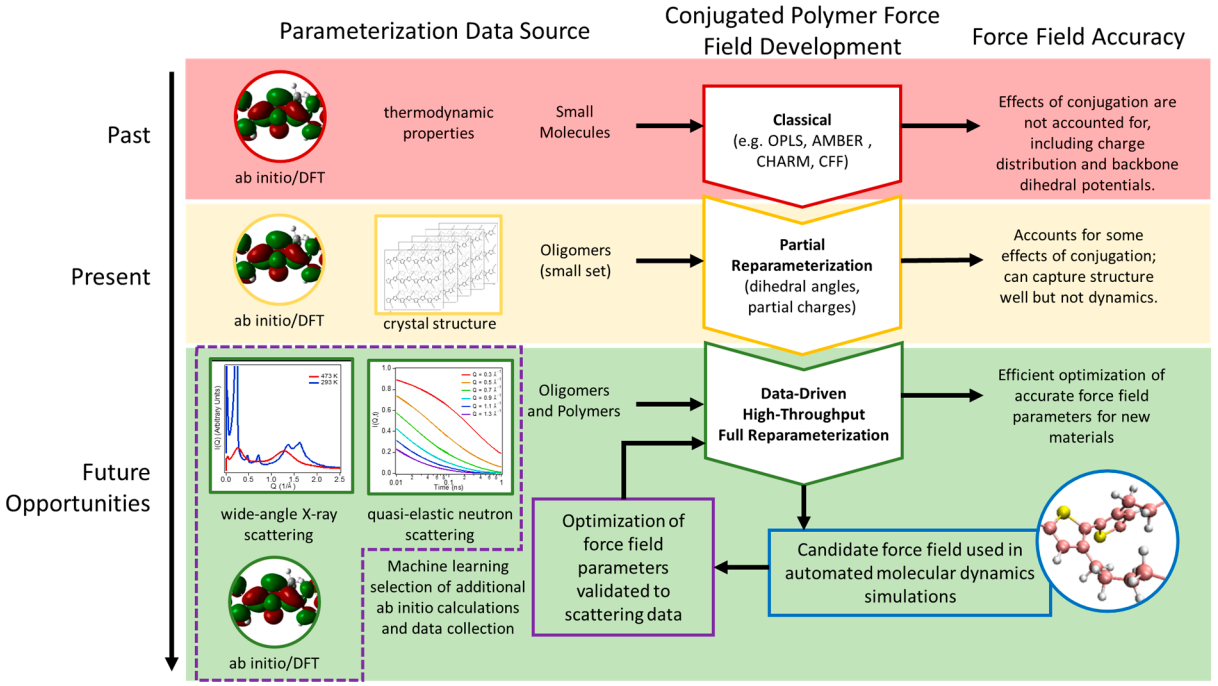


**Figure 1.** Schematic demonstrating the varying levels of FF development for CPs, from past classical models, the current partially reparametrized FFs, and to future opportunities in high-throughput development of accurate FFs using machine learning and neutron and X-ray scattering data.

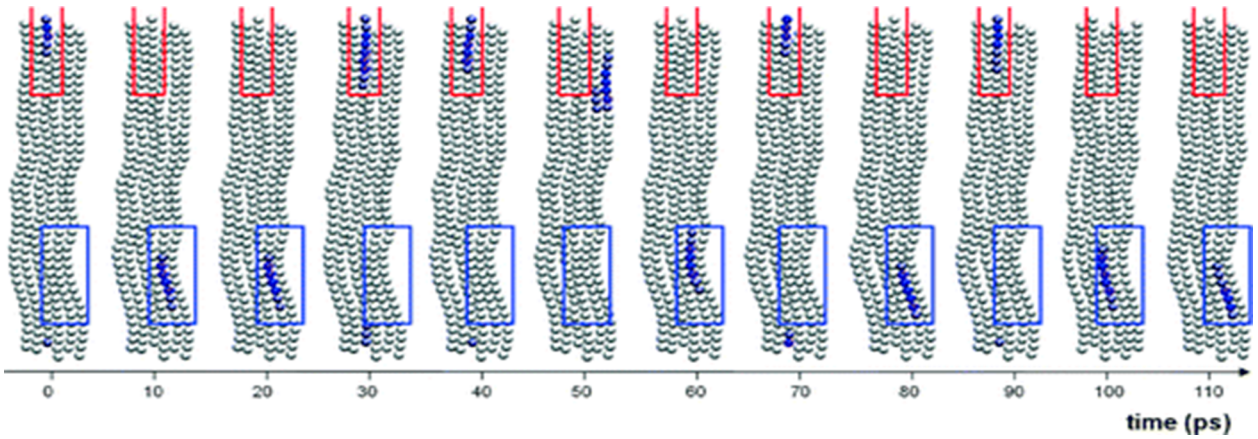


**Figure 2.** Highest-occupied molecular orbital (HOMO) density localization for P3HT chains simulated with a regioregularilty of 56% as a function of MD simulation time. During the simulation, the localization of the HOMO orbital density frequently fluctuates between one of two regions, which are shown by the red and blue boxes. Figure reprinted with permission from reference 17. Copyright 2011 American Chemical Society.

electronic performance with both experimental and molecular modeling approaches. Both experimental and simulation approaches can be helpful in this pursuit, but here, we provide our perspectives on a powerful combined approach involving quantitative comparisons between atomistic molecular dynamics (MD) simulations and neutron and X-ray scattering. Together, these methods provide insight into this structure–function relationship that neither approach could provide on their own and can help to develop physically accurate MD force fields (FF) for CPs as shown in Figure 1.

Both quantum and classical molecular modeling approaches provide useful tools for studying the relationship between morphology and performance in CPs at length scales on the order of picometers to millimeters and at time scales on the order of femtoseconds to milliseconds. Bond vibrations, electronic orbitals, lowest-energy molecular conformations, and nonbonded interactions can be captured with highly accurate quantum-mechanical ab initio calculations and density functional theory (DFT), but these require a compromise with feasible simulation size and computational expense. Rouse motions, atomic structure and dynamics, and chain conformation (e.g., radii of gyration, persistence length) can be captured by use of atomistic MD simulations, which utilize classical approximations of bonded and nonbonded interactions with quantum-mechanical origins to enable larger-scale simulations and to access longer time and length scales with some penalty to accuracy. Finally, larger-scale processes such as chain reptation and diffusion can be probed with coarse-grained MD simulations, which further bundle atoms into single moieties with interactions that approximate their summed behavior and result in the greatest compromise of accuracy to reach the longest time and length scales.

Both classical MD and ab initio methods have been used widely to understand charge transport mechanisms in CPs.


https://doi.org/10.1021/acspolymersau.1c00027
ACS Polym. Au 2021, 1, 134–152

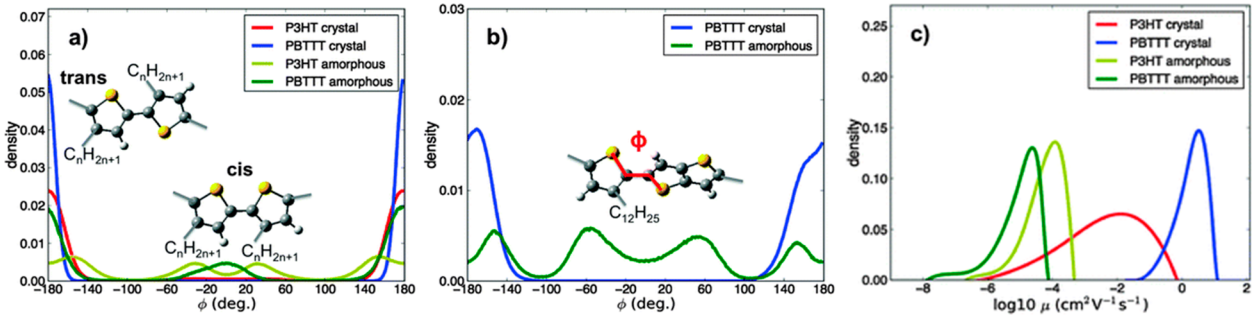


**Figure 3.** Distributions of dihedral angles (a) between thiophene rings in P3HT and PBTTT simulations and (b) between thiophene rings and thienothiophene units in PBTTT simulations. (c) Distribution of hole mobilities from simulations of crystalline and amorphous phases of P3HT and PBTTT calculated using Marcus theory. Confidence intervals could not be shown for reprinted figures. Figures were adapted with permission from reference 18. Copyright 2015 The Royal Society of Chemistry.

McMahon et al. were interested in the relationship between structural regioregularity defects and the electronic density of states in crystalline poly(3-hexylthiophene) (P3HT).[17] The researchers used efficient MD simulations to obtain "snapshot" structures across long time scales that were then used as the molecular conformations in DFT calculations of electronic structure, as shown in Figure 2, to study localized "trap states" that directly influenced charge transport. This combined approach enabled the study of this behavior with a high accuracy at time scales that would not be achievable with one technique alone. The team found good agreement between the computed electronic behavior of these materials when compared with the experimentally determined field-effect mobility of OFETs prepared from P3HT with varying degrees of regioregularity. These structural defects were found to have a minimal effect on the charge traps in the material, as the traps are commonly found in regions of high planarity, i.e., high regioregularity, contrary to a previously common belief. Alberga et al. employed atomistic MD simulations of crystalline and amorphous phases of P3HT and poly(2,5-bis(3-alkylthiophen-2-yl)thieno[2,3-*b*]thiophene) (PBTTT) as well as Marcus theory to understand the relationship between the molecular structure and charge mobility for these materials.[18] They found that while side chains do not play a direct role in charge transport mechanisms, they influence the distribution and fluctuation of backbone dihedrals, which are directly tied to charge mobility through Marcus theory. In the crystalline phase of PBTTT, side-chain interdigitation is found to improve charge mobility when compared to crystalline P3HT. However, the higher density of side chains along the P3HT backbone improves the stability of backbone dihedrals (i.e., lower fluctuations) in the amorphous phase resulting in improved charge mobility when compared to amorphous PBTTT. Shown in Figure 3 are the distributions of the relevant backbone dihedral angles and resulting hole mobility distributions for amorphous and crystalline phases of P3HT and PBTTT. Tapping et al. used large-scale simulations that employed a coarse-grained model of P3HT chains in solution, demonstrating extended conformations in good solvent and nanofiber formation in a moderate solvent.[19] Then, by mapping back to an atomistic representation of the molecules, the team could use quantum-mechanical calculations to understand the movement of excitons from the surface of P3HT aggregates to the crystalline core, which could trap excitons and prevent them from reaching donor−acceptor interfaces in devices. This emphasizes the importance of understanding morphology−performance relationships across multiple time and length scales to enable tuning of CP materials for specific applications and to improve efficiency of organic electronic devices.

In all these works, the choice of the MD FF directly influences the structures that are used for subsequent ab initio calculations to understand charge transport. FF parameters for new CPs are often determined either via ab initio approaches or by comparing to empirically determined physicochemical properties. However, the methods, algorithms, measurements, and specific material properties that are used to develop FFs could drastically influence the accuracy and predictive qualities of the resulting simulations (Figure 1). In this work, we review existing MD FFs for CPs, including their parametrization and validation. We find that although there has been some agreement in the literature about the importance of backbone dihedral torsion potentials and partial charges in FFs parametrized for CPs, there has been little work expanding CP FFs outside of the polythiophene family. This should not suggest that there is a reduced need for new FFs but rather that large-scale parametrization is a complex and arduous process with significant challenges associated with the large chemical diversity of CPs. Fortunately, modern advances in data science, high-performance computing, and computational chemistry promise to accelerate progress. In the following section, a discussion on experimental approaches used in FF validation is introduced with an emphasis on the integration of neutron and X-ray scattering methods. These tools are particularly advantageous for validation, because they probe material structure and dynamics on the same length and time scales as MD simulations. Moreover, neutron scattering also enables the use of contrast variation, a tool that can help researchers to focus on specific features within a molecule or material. Our past work employing contrast variation found that existing FFs for P3HT fail to capture characteristic backbone motions in regiorandom P3HT that are relevant to charge transport mechanisms.[20] Thus, we further propose that the adjustment of nonbonded parameters in CP FFs must be considered to improve future molecular models. DFT calculations suggest that classical parameters, which are frequently adopted without adjustment from generalized FFs (e.g., OPLS), do not adequately capture the effects of conjugation along the CP backbone. Finally, we provide a discussion and outlook on how data science could open up new opportunities for high-throughput FF parametrization in the future, not only to develop FFs for new CPs but also to provide an efficient and systematic process to improve model parameters.


https://doi.org/10.1021/acspolymersau.1c00027
*ACS Polym. Au* 2021, 1, 134−152

## II. CURRENT FORCE FIELDS OF CONJUGATED POLYMERS

An MD simulation uses a potential energy function and corresponding set of parameters to describe all bonded and nonbonded interactions between atoms. The functional form (i.e., potential equations), parameters, and method used for development (i.e., parametrization) can vary and will affect both the accuracy and applicability of the resulting FF. By integrating the potential energy function, the force felt by every atom due to its bonded and nonbonded interactions with nearby atoms can be used to update each its position and velocity at every time step during the simulation. For CPs specifically, many of the reparametrized FFs use a Class I functional form to describe the bonded and nonbonded potential energies, which is represented by[21−23]

$$V = V_{bonded} + V_{nonbonded} \tag{1}$$

$$\begin{aligned} V_{bonded} = {} & \Sigma_{bonds}\frac{1}{2}K_{b,ij}(b_{ij} - b_{o,ij})^2 + \Sigma_{angles}\frac{1}{2}K_{\theta,ijk}(\theta_{ijk} - \theta_{o,ijk})^2 \\ & + \Sigma_{impropers}\frac{1}{2}K_{\zeta,ijkl}(\zeta_{ijkl} - \zeta_{o,ijkl})^2 \\ & + \Sigma_{dihedrals}\frac{1}{2}K_{\phi,ijkl}(1 + \cos(n\phi_{ijkl} - \delta_n)) \end{aligned} \tag{2}$$

$$V_{nonbonded} = \Sigma_{pairs}\left[4\epsilon_{ij}\left(\left(\frac{\sigma_{ij}}{r_{ij}}\right)^{12} - \left(\frac{\sigma_{ij}}{r_{ij}}\right)^{6}\right) + \frac{q_i q_j}{\kappa r_{ij}}\right] \tag{3}$$

where $V$ is the total potential energy of bonded ($V_{bonded}$) and nonbonded ($V_{nonbonded}$) components to the force field. In the bond ($\Sigma_{bonds}$), angle ($\Sigma_{angles}$), and improper dihedral ($\Sigma_{impropers}$) contributions, $K$ is the bond, angle, and improper angle spring constant for bonds $b_{ij}$, angles $\theta_{ijk}$, and improper angles $\zeta_{ijkl}$, respectively. The equilibrium bond length, angle, and improper angle are represented by $b_{o,ij}$, $\theta_{o,ijk}$, and improper angle $\zeta_{o,ijkl}$. The dihedral contribution ($\Sigma_{dihedrals}$) is defined by the dihedral spring constant, $K_{\phi,ijkl}$, the dihedral angle between four linearly bonded atoms, $\theta_{ijk}$, and the phase, $\delta_n$. The nonbonded potential includes a pair potential, shown here by the 12/6 Lennard-Jones potential, and Coulombic interactions. $\epsilon_{ij}$, $\sigma_i$, and $\sigma_j$ are the Lennard-Jones parameters, $q_i$ and $q_j$ are the atomic partial charges, $\kappa$ is the dielectric constant, and $r_{ij}$ is the distance between nonbonded atoms $i$ and $j$.

A review of FFs that have been reparametrized for CPs is provided in Table 1 with a focus on polythiophenes, because these materials have provided a model system of study for the community. FFs for CPs utilize a classical FF as the base and make modifications to the parameters thought to be most influenced by conjugation. Commonly selected base classical FFs include the Optimized Potentials for Liquid Simulations All-Atom (OPLS-AA) FF,[24−26] the Generalized Assisted Model Building with Energy Refinement (AMBER) FF (GAFF),[27] the Chemistry at Harvard Macromolecular Mechanics (CHARMM) FF,[28] the Groningen Molecular Simulation (GROMOS) FF,[29,30] and the molecular mechanics (MM3) FF.[31−33] The OPLS-AA FF follows closely the functional form provided above and is a well-developed classical set of parameters for a wide range of organic liquids and proteins. GAFF was developed as a generalized model for organic molecules to supplement the AMBER FF originally designed for proteins and nucleic acids. Its advantage is a limited set of atom types that can be combined with the empirically derived algorithms to create a full set of parameters for specific molecules based on their bonded geometry. CHARMM and GROMOS were both developed for biological materials but also refer to simulation software that includes tools to parametrize FFs for new molecules using their built-in methodologies and parameters. The MM3 FF uses a similar form to the one presented in eqs 1−3 but also includes cross-interaction terms of stretch−bend, torsion stretch, torsion−bend, and bend−bend to represent the motions of bonded atoms more accurately and is classified as a Class II FF. It was developed for aliphatic hydrocarbons and a collection of small molecules, including thiophene derivatives. Classical FFs are commonly parametrized to reproduce crystal structures, heats of formation, heats of vaporization, density, or ab initio intermolecular interactions.[24−27,31−33] After relevant parameters were selected from the classical models, Table 1 shows that the most frequently reparametrized interactions for CPs include the electrostatic interactions (partial charges) and torsion potentials along the backbone, with only a couple models making variations to bond and angle contributions or the nonbonded Lennard-Jones interactions. We also find that there is a wide range of approaches used in the reparameterization process. For example, many differ on the representative oligomers and levels of theory that are used for ab initio calculations and the empirical and theoretical parameters that are used for validation.

Despite the range of approaches that have been used, there is widespread agreement among the FFs in Table 1 that the dihedral torsion potential between two monomers along the backbone will be greatly affected by conjugation and needs to be reparametrized. The modified torsion potential is determined via dihedral angle scans of relevant oligomers using ab initio simulations. After an initial planar geometry optimization of the molecule, energy calculations are performed as the central dihedral angle is "stepped" through either a half or full rotation. These scans are performed with or without side chains (to reduce computational expense) and with a range of ab initio theories. The early models from Marcon et al. found that the torsion potential barrier was overestimated in the classical MM3 FF when compared with potentials derived from ab initio calculations.[34] Moreover, the potential energy was noticeably lower for the *cis*-conformation of thiophene rings in the classical model, but calculations at the MP2/aug-cc-pVTZ level of theory for 2,2′-bithiophene show a smaller energy difference with a slight preference for the *trans*-conformation. Widge et al. point out, however, that regardless of a preference for a *trans*-conformation evident from ab initio calculations in vacuum, the surrounding medium can also influence the final dihedral distribution in the system.[37] They compared MD simulations of P3HT and P3EHT in an implicit solvent of either water (poor solvent) or hydrocarbons (moderate solvent) and observed that more favorable solvent−polymer interactions resulted in a preference for *trans*-conformations in the hydrocarbon as compared to water. Moreover, they observe preferred geometries that are slightly shifted from perfectly planar conformations by approximately 50−60°, which has been observed in prior polythiophene simulations from other groups. Schwarz et al. also emphasize that the chain length of the oligomer used in parametrization of the inter-ring torsion potential should be carefully considered, as longer oligomers would result in greater electron delocalization and higher torsion potential.[42] Bhatta et al. performed a thorough analysis of these torsion potentials


https://doi.org/10.1021/acspolymersau.1c00027
ACS Polym. Au 2021, 1, 134−152

**Table 1. Selected Atomistic Molecular Dynamics FFs for CPs with a Focus on Polythiophenes**[a]

| force field | year | polymer(s) | base classical force field | reparametrized interactions | reparameterization molecules | ab initio level of theory | force field validation approach |
|---|---|---|---|---|---|---|---|
| Marcon et al.-OT[34] | 2004 | oligothiophenes | MM3[31−33] | inter-ring torsion potential, partial charges, van der Waals interactions | polythiophene dimer and tetramer, dithienothiophene dimer, perfluorinated polythiophene hexamer | MP2/aug-cc-PVTZ, B3LYP/6-31G** | crystal structure (X-ray diffraction) |
| Marcon et al.-TT[35] | 2006 | tetrathiophene | MM3,[32] OPLS-AA[24] | inter-ring torsion potential, partial charges | polythiophenes 4−6 monomers long, varied side-chain groups | MP2/aug-cc-pVTZ, electrostatic potential fitting | crystal structure (X-ray diffraction); heat of sublimation |
| Marcon et al.-OF[36] | 2006 | oligofluorenes | MM3[31,33] | inter-ring torsion potential, partial charges, van der Waals interactions | fluorene dimer | B3LYP/6-311G* and B3LYP/6-311++G**, electrostatic potential fitting | crystal structures of fluorene and fluorenone (X-ray diffraction) |
| Widge et al.[37] | 2007 | poly(3-hexylthiophene) (P3HT), poly(3-(2′-ethyl) hexylthiophene) (P3EHT) | generalized AMBER FF (GAFF)[27] | inter-ring torsion potential, partial charges, inter-ring bonds and angles | polythiophene dimers and pentamers | HF/6-31G* | molecular geometry (X-ray powder diffraction, gas phase electron diffraction, microwave rotational spectroscopy, solution NMR, gas phase fluorescence); ab initio molecular geometry, solubility trends in moderate and poor solvent |
| Moreno et al.[23] | 2010 | polythiophenes | OPLS-AA[24,25] | inter-ring torsion potential, thiophene ring−alkyl side-chain torsion potential, partial charges | oligothiophenes with length of 4−6 monomers | elestrostatic potential fitting at B3LYP/6-311G** | crystal structures of polymer and oligomer polythiophenes with and without side chains from Cambridge Structural Database[38] |
| DuBay et al.[39] | 2012 | poly(2-methoxy-5-(2′-ethylhexyloxy)-*p*-phenylenevinylene) (MEH-PPV), poly(3-hexylthiophene) (P3HT) | OPLS-AA[25] | inter-ring torsion potential, bond-stretching, angle-bending, steric repulsion interactions | bithiophene, stilbene | LMP2/cc-pVTZ(-f) and B3LYP/6-31++G** (inter-ring torsion potential) | persistence length; *in silico* dihedral angle and conjugation length distributions |
| Bhatta et al.[40] | 2013 | poly(3-hexylthiophene) (P3HT) | OPLS-AA,[24] Marcon et al.-TT[35] | inter-ring torsion potential, partial charges, some bond and angle parameters | decamer | B3LYP/6-31+G**, MP2/6-31+G** | mass density, melting temperature, glass-transition temperature, surface tension |
| Łużny et al.[41] | 2013 | poly(alkylthiophene)s | OPLS-AA[24,26] | hierarchical approach of thiophene bonds and angles, inter-ring torsion potential, partial charges | thiophene, 2,2′-bithiophene, oligothiophenes of lengths 2, 4, 6, and 8 monomers, tetra(3-butylthiophene), alkanes | B3LYP/6-31G* and B3LYP/6-311G* | crystal structure (X-ray diffraction) |
| Schwarz et al.[42,43] | 2013 | poly(3-hexylthiophene) (P3HT) | OPLS-AA[24] | inter-ring torsion potential, partial charges, bond lengths, angles | tetrathiophene, 3-methylthiophene 14mer | MP2/aug-cc-pVTZ | mass density, crystal structure, heat of sublimation |
| Jackson et al.[44] | 2015 | see Figure 5 | OPLS-AA[24] | intramonomer torsion potential, bonds, angles, stretching, bending, partial charges | monomers, dimers | B3LYP/6-31+G**, RI-MP2/cc-pVTZ | X-ray diffraction |
| Wildman et al.[45] | 2016 | polyfluorenes, polythiophenes | OPLS-AA[24,46−51] | inter-ring torsion potential, partial charges | dimer | CAM-B3LYP/6-31G*, CAM-B3LYP/cc-pvTZ | persistence length, end-to-end length |
| Lee et al.[52] | 2017 | isoindigo-thienothiophene (ITTT) | CHARMM[28] | partial charges, intramonomer torsion potentials | monomer in presence of solvent | MP2/6-31G* | not available |
| Sundaram et al.[53] | 2020 | diketopyrrolopyrroles | GROMOS 54A7,[30] GROMOS 96 FF[29] | bonds, angles, dihedrals, partial charges | monomer, dimer | B3LYP/def2-TZVP | solution conformation, glass-transition temperature |
| Kıbrıs et al.[54] | 2021 | poly-*N*,*N*,*N*-trimethyl-3-(4-methylthiophen-3-yl)oxy) propan-1-aminium (CPT) | CHARMM[55] | partial charges, dihedrals, bonds, angles | monomer, dimer | MP2/6-31G*, HF/6-31G* | molecular mechanics and quantum-mechanics calculations, UV−vis spectroscopy (absorption spectra responses) |
| Michaels et al.[56] | 2021 | poly(3,4-ethyl-enedioxythiophene) (PEDOT) | generalized AMBER FF (GAFF)[27] | partial charges, bonds, dihedrals, | hexamer | ωB97x-D/jun-cc-pVDZ, HF/6-31G* | ab initio calculations at DF-DSD-PBEP86/jun-cc-pV(T+d)Z |



https://doi.org/10.1021/acspolymersau.1c00027
ACS Polym. Au 2021, 1, 134−152

Table 1. continued

[a]Many FFs are developed by selected a classical FF as the base and modifying relevant parameters that are expected to deviate for CPs. Included in the table are these reparametrized interactions as well as the molecules used in their parameterization process. Finally, we note the ab initio level of theory used during this process as well as the experimental and theoretical validation metrics chosen by the researchers.

for P3HT and polythiophene (no side chains) at a range of lengths from 2 to 12 monomers, as shown in Figure 4.[57] They find that the potential converges after an octamer length for P3HT and that the inclusion of side chains results in a lower potential energy barrier due to nonbonded interactions of nearby side chains in the planar configurations. In our previous work, we also compared this backbone dihedral potential across five different FFs from three different works and found that they all differed not only in the potential energy barrier at 90° but also in the preferred *trans*- or *cis*-conformation of the backbone thiophene rings, as shown in Figure 4.[20] This resulted in a significant difference in the distribution and degree of fluctuation in large-scale simulations of regiorandom P3HT using these models. Similarly, the different levels of theory and parametrization approaches across the works presented in Table 1 resulted in sets of partial charges with minimal consistency, both in sign and magnitude, across the models. As shown in our previous work,[20] this also influenced molecular structure and dynamics relevant to charge transport calculations, i.e., Marcus theory.

By far, CP FF parametrization in the literature has focused on the family of polythiophenes. These molecules are relatively simple molecules that have been well-studied experimentally in the literature, making them an ideal model system for parametrization and validation. Some of the works, however, have also explored FFs for molecules outside of the polythiophene family,[36,39,44,45,52,53,56] including the work of Jackson et al. that provided FF parameters consistent with OPLS-AA for the 15 different conjugated polymers that are shown in Figure 5 and studied their solution conformation and behavior to learn more about the relationship between structure and performance.[44] They found that more planar backbones tend to form more ordered conformations (i.e., rod, stacked rod, and toroid), which lead to more $\pi$-stacking and to improved charge transport. However, the researchers note that other factors, such as side chains, can also influence this relationship and other structural descriptors, such as dihedral distributions. Therefore, the backbone torsion potentials were not a clear indication of the resulting dihedral distributions of the simulations. Furthermore, the researchers conclude that longer range ordering is not necessarily tied to improved performance, but rather, the local polymer ordering is more important. The parametrization procedure of Jackson et al. was noted as an effective approach to generating FFs for other CPs in future work, as the methods used were of modest computational cost.

Other works have proposed generalized methodologies for CP FF development, including Wildman et al.[45] and Łużny et al.,[41] and while the details vary, they all agree upon the importance of torsion potentials and partial charges. Still, slight variations in each approach resulted in a wide range of model parameters across available FFs for CPs. Nevertheless, all groups created systems that were validated to experimental or theoretical parameters and that provided valuable *in silico* insight into their materials. This highlights the difficult nature of capturing the complex quantum-mechanical interactions in CPs using a classical atomistic approximation. Moreover, we find that parametrization efforts for CP FFs have slowed in recent years due to the high computational costs and challenges that were encountered for even the simplest polythiophenes. For more complex molecules, researchers need to rely on classical models or FF toolkits based on classical sets to generate FF parameters, as added molecular


https://doi.org/10.1021/acspolymersau.1c00027
ACS Polym. Au 2021, 1, 134−152

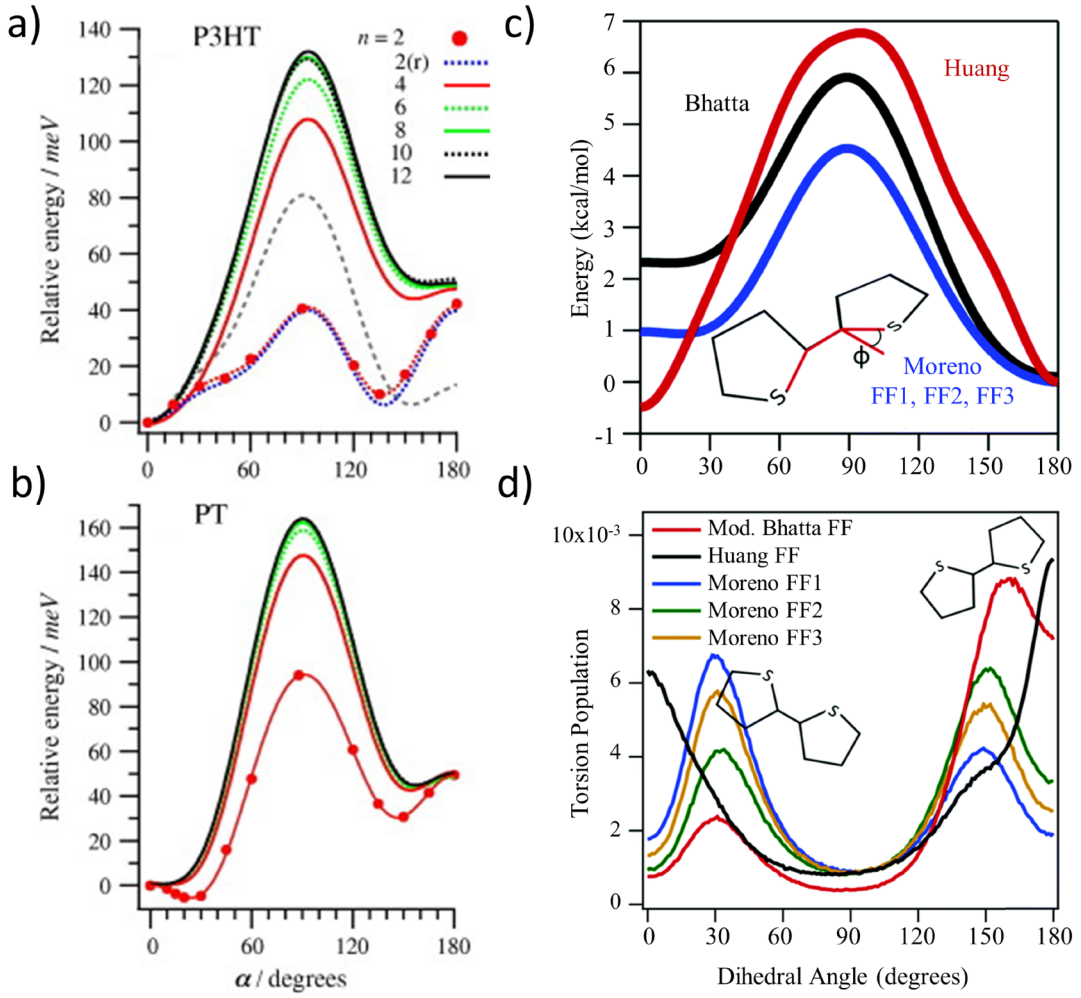


**Figure 4.** (a,b) Backbone dihedral torsion potential for P3HT and oligothiophenes of varying length calculated at the B3LYP/6-31+G(d,p) level of theory. Markers are shown for the dimer to demonstrate at which torsional angles the energy was calculated. The gray dashed line in panel (a) was calculated using dispersion corrections at the B3LYP-D2/6-31+G(d,p) level of theory. The 2(*r*) line in panel (a) is representative of additional geometry optimization at each step. A *trans*-conformation of the thiophene rings corresponds to a dihedral angle of 0° in these plots. (c) Backbone dihedral torsion potential for P3HT from three different FFs including Moreno et al.[23] (Moreno FF1, FF2, and FF3), Bhatta et al.[40] (Mod. Bhatta FF), and Schwarz et al.[42,43] (Huang FF). (d) Backbone torsion populations from MD simulations of regiorandom P3HT with a chain length of 60 monomers using the same selection of FFs. A *trans*-conformation of the thiophene rings corresponds to a dihedral angle of 180° in panels (c) and (d). Confidence intervals could not be shown for reprinted figures. Figures in panels (a) and (b) were reprinted with permission from reference 57. Copyright 2012 Elsevier B.V. Figures in panels (c) and (d) were reprinted with permission from reference 20. Copyright 2019 The Royal Society of Chemistry.

complexity exponentially increases computational cost of the parametrizations reviewed above. Regardless, we emphasize that the choice of FF, or choice of parametrization method(s), level of theory, and basis molecules as well as the selected validation metrics will all impact the resulting *in silico* behavior of the MD simulations and their accuracy with respect to physical systems at different time and length scales.

## III. EXPERIMENTAL VALIDATION OF FORCE FIELDS

The choice of a validation metric can affect the perceived accuracy of FFs at specific time and length scales, which can also influence their applicability for specific cases. Figure 6 shows a selection of experimental and computational tools that have been used to study polymeric properties at different time and length scales. Molecular fluctuations, especially along the conjugated backbone, are incredibly influential to charge transport in CPs as described by Marcus theory. However, we note that most parametrized CP FFs are only validated against thermophysical or structural material properties. Quasielastic neutron scattering (QENS) is an underutilized but powerful approach to validating CP FFs, as the technique covers the same time and length scales of molecular simulations. Moreover, QENS and MD simulations can be used together as a powerful combined approach to understand molecular fluctuations on the order of picoseconds to nanoseconds along the backbone and to describe how they influence charge transport in CPs beyond what experimental approaches can provide on their own. In this section, we first provide a concise review of both elastic and inelastic neutron and X-ray scattering methods and how they have been used in the past to explore structural and dynamic properties of CPs. We then provide metrics that can be used to directly compare between experimental scattering results and molecular dynamics simulations. Finally, we provide a discussion on the advantages of using QENS as a validation metric for atomistic MD FFs.


https://doi.org/10.1021/acspolymersau.1c00027
ACS Polym. Au 2021, 1, 134−152

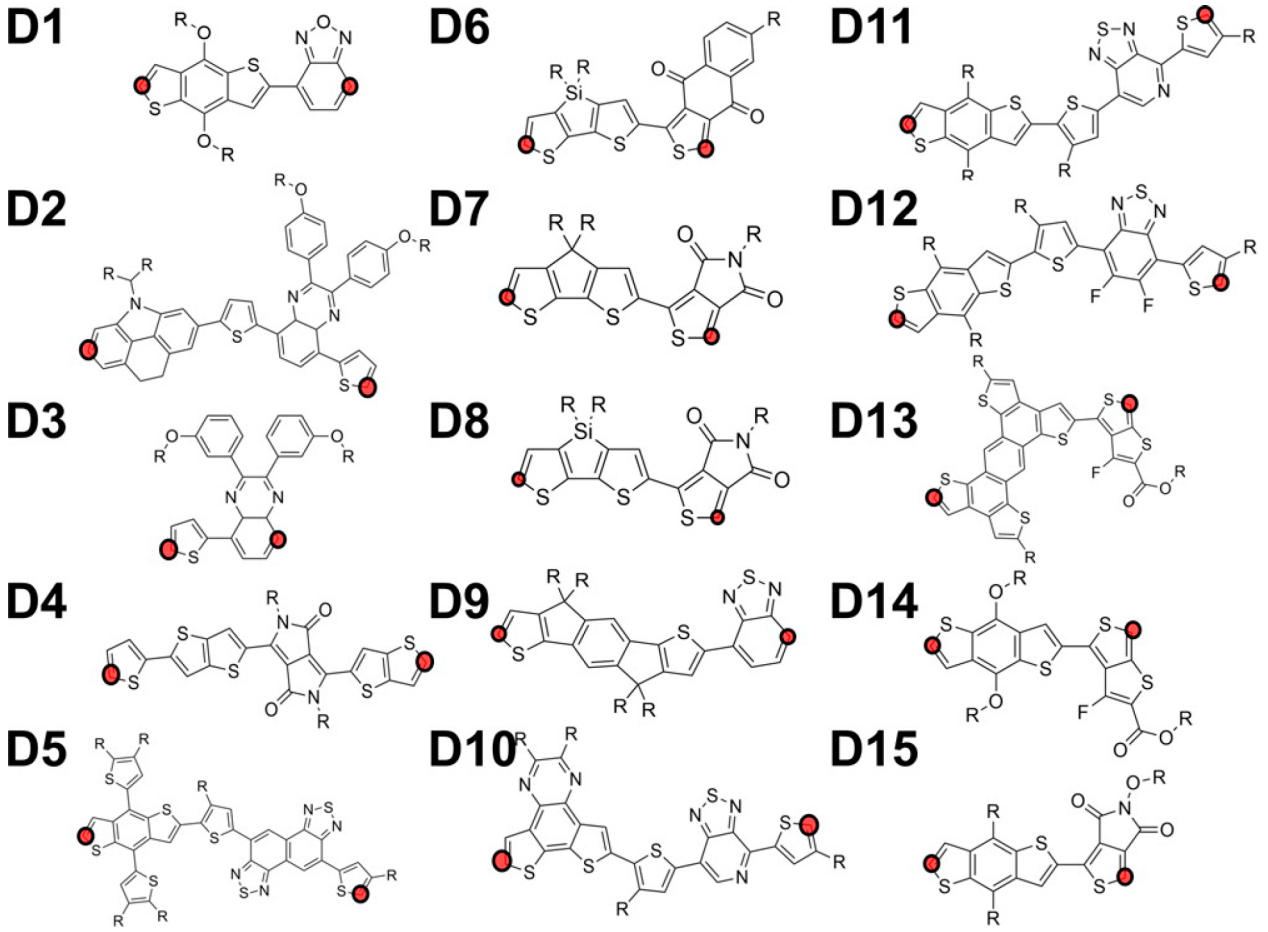


**Figure 5.** Conjugated monomers used in the FF development from the work of Jackson et al. The red markers indicate the atom bonded to the next monomer in the polymer form. Figure reprinted with permission from reference 44. Copyright 2015 American Chemical Society.

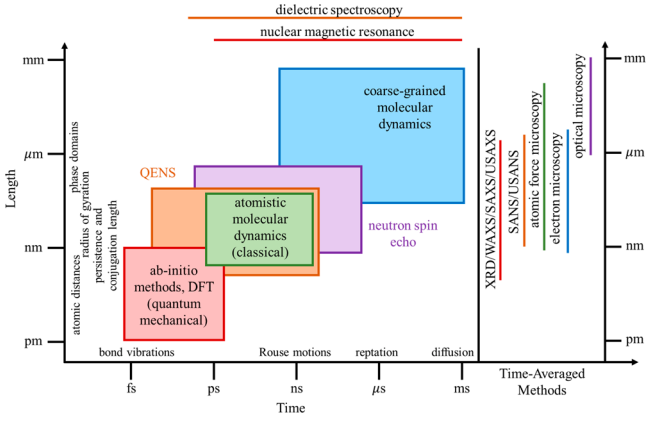


**Figure 6.** Time and length scales of experimental and computational methods compared to polymer properties.

## A. Review of Elastic and Inelastic Scattering X-ray and Neutron Scattering Theory

The scattering techniques of QENS, small-angle X-ray or neutron scattering (SAXS, SANS), and wide-angle X-ray scattering (WAXS) may vary in instrumentation and in the material structure and dynamics that they can probe, but they all make use of the same scattering fundamentals. An incident beam of neutrons or X-rays is passed through a material, and the small fraction that scatter at a particular angle, $\theta$, are analyzed to provide information about the molecular level structure and dynamics. Elastic scattering methods, including SANS, SAXS, and WAXS, assume that the scattered beam only changes in momentum (direction) and can be related to structural features at characteristic length scales, $d^*$, in the material through the scattering vector, $q$[58]

$$q = \frac{4\pi}{\lambda}\sin\left(\frac{\theta}{2}\right) \tag{4}$$

$$q^* = \frac{2\pi}{d^*} \tag{5}$$

where $q$ is the difference between the scattered and incident beam vectors, $\lambda$ is the wavelength of the incident beam, and $\theta$ is the scattering angle between the incident beam and scattered beam. Inelastic scattering methods, including QENS, utilize both the momentum and energy change of the scattered beam to collect information about the molecular dynamics of the material. The scattering vector, $q$, and the energy change, $\Delta E$, can be related to the incident and scattered beams, $k_i$ and $k_f$, through the following equations[58]

$$q = k_i^2 + k_f^2 - 2k_i k_f \cos(\theta) \tag{6}$$

$$\Delta E = \frac{h^2}{4\pi m}(k_f^2 - k_i^2) \tag{7}$$

where $\Delta E$ is the energy change, $h$ is Planck's constant, and $m$ is the neutron mass.


https://doi.org/10.1021/acspolymersau.1c00027
ACS Polym. Au 2021, 1, 134−152

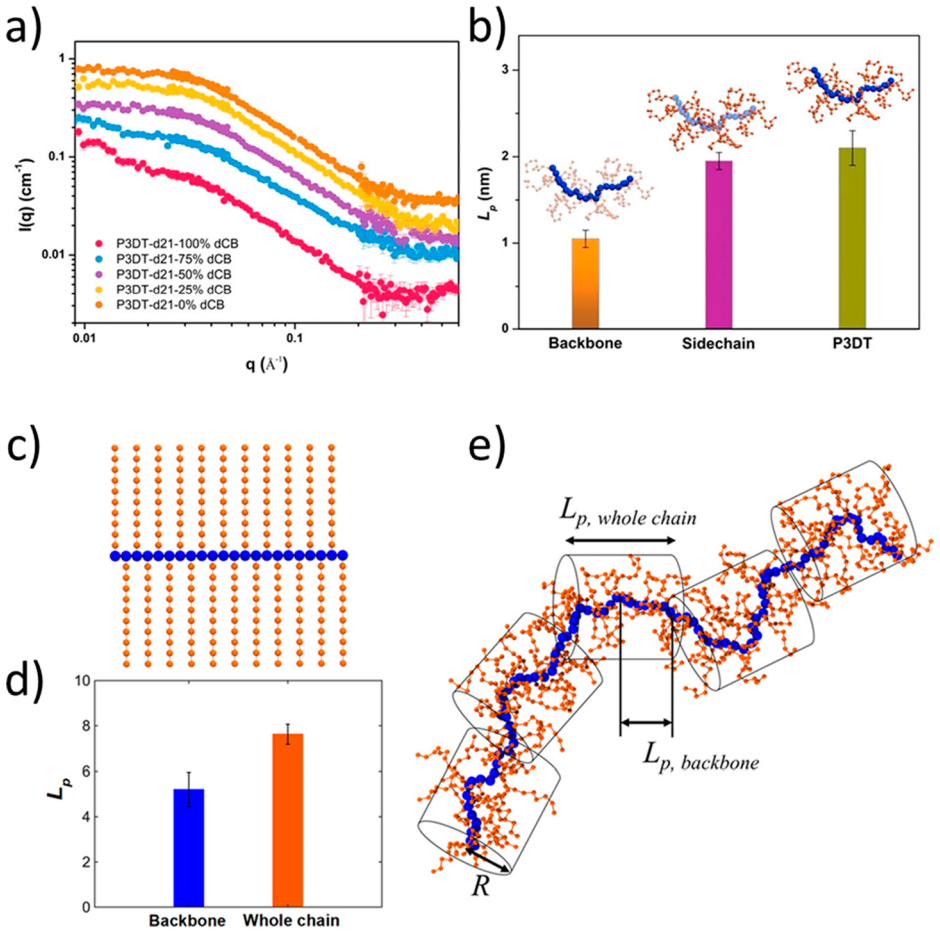


**Figure 7.** (a) SANS data of P3DT-d21 (deuterated side chains) at varying ratios of deuterated chlorobenzene (dCB) and hydrogenated chlorobenzene to highlight structure of the backbone and side chains. (b) Persistence lengths ($L_P$) of the backbone, side chain, and whole chain of P3DT determined using contrast variation of the molecule and solvent. (c) Representation of the coarse-grained molecules used in coarse-grained MD simulations of P3DT. The backbone was represented by 100 beads, and each side chain was represented by 10 beads. (d) Persistence length in reduced Lennard-Jones units of the backbone and whole chain as determined from coarse-grained MD simulations. (e) Molecule from the MD simulations that shows the chain broken up into persistence segments (cylinders), and notations for the persistence lengths of the whole chain and backbone. Confidence intervals could not be shown for reprinted figures. Figure reprinted with permission from reference 65. Copyright 2020 American Chemical Society.

X-rays and neutrons interact with materials differently: X-rays with the electron cloud and neutrons with the atomic nucleus. This interaction strength is quantified using the scattering length, $b$, and the scattering cross section, $\sigma$, which can be thought of as controlling the probability of a scattering event.[58] Therefore, the scattering length density (SLD) of a material is determined by both the atoms present and the incident radiation, i.e., neutrons or X-rays. The total scattering cross section includes both coherent and incoherent scattering. Identical spatially correlated SLDs result in coherent scattering, which includes information about the internal structure or pair-correlated motions. Incoherent scattering, however, arises from a distribution of scattering lengths and includes information about self-correlated motions.[58−61] Elastic scattering techniques measure the differential cross section, which is defined as the neutrons scattered per scattering angle, to extract structural information about a material. This differential cross section can be broken down into its coherent and incoherent contributions by the following formulas[58,59]

$$\left[\frac{\delta\sigma}{\delta\Omega}(q)\right]_{coh} = \langle b\rangle^2 \Sigma_{j,k=1}^{N} \langle e^{iq\cdot r_{jk}}\rangle \tag{8}$$

$$\left[\frac{\delta\sigma}{\delta\Omega}\right]_{inc} = N(\langle b^2\rangle - \langle b\rangle^2) \tag{9}$$

$$\frac{\delta\sigma}{\delta\Omega}(q) = \left[\frac{\delta\sigma}{\delta\Omega}(q)\right]_{coh} + \left[\frac{\delta\sigma}{\delta\Omega}\right]_{inc} \tag{10}$$

where $\sigma_{coh}$ and $\sigma_{inc}$ are the coherent and incoherent cross sections, respectively, $b$ is the scattering length, $\Omega$ is the scattering angle, $N$ is the total number of particles, and $r_{jk}$ is the position vector between particles $j$ and $k$. This scattering intensity as a function of the scattering vector, $q$, can be fit with a range of models to quantify the shapes and sizes of structures present in the sample, and we refer the reader to the work of Hammouda et al.[62] for a thorough review of SANS theory and analysis. Inelastic scattering techniques measure the double-differential cross section, which is defined as the neutrons scattered per solid angle and per energy change,[58,59,61] to extract information about a material's dynamic fluctuations. QENS techniques specifically are sensitive to small energy changes caused by molecular rotations and translations.[58] This double-differential cross section can also be broken down into


https://doi.org/10.1021/acspolymersau.1c00027
ACS Polym. Au 2021, 1, 134−152

its coherent and incoherent contributions by the following formulas[59]

$$\frac{\delta^2\sigma}{\delta\Omega\delta\omega} = N\frac{k_f}{k_i}((\langle b^2\rangle - \langle b\rangle^2)S_{inc}(q,\omega) + \langle b\rangle^2 S_{coh}(q,\omega)) \tag{11}$$

$$S_{inc}(q,\omega) = \frac{1}{2\pi N}\int \mathrm{d}t\langle \Sigma_j e^{i(q\cdot(r_j(t)-r_j(0))-\omega t)}\rangle \tag{12}$$

$$S_{coh}(q,\omega) = \frac{1}{2\pi N}\int \mathrm{d}t\langle \Sigma_{j,k} e^{i(q\cdot(r_k(t)-r_j(0))-\omega t)}\rangle \tag{13}$$

where $\omega$ is frequency (related to neutron energy), $t$ is time, and all other variables remain as previously defined. QENS data is most frequently collected in the energy domain, and so, the data are converted to the time domain with a Fourier transform, which also enables deconvolution with the instrument's resolution[61]

$$I(q,t) = \frac{\int S(q,\omega)e^{i\omega t}\mathrm{d}\omega}{\int R(q,\omega)e^{i\omega t}\mathrm{d}\omega} \tag{14}$$

where $R(q,\omega)$ is the resolution function. The elastic scattering signal of a QENS measurement also provides information about the different phases of a material's dynamics. In "elastic mode" or "fixed window scans", the elastic scattering intensity is tracked as a function of temperature, which can be converted into a mean squared displacement using the formula for the Debye−Waller factor[63]

$$S(q,\omega=0) = e^{-q^2\langle u^2\rangle/3} \tag{15}$$

where $\langle u^2\rangle$ is the mean squared displacement.

The differing interactions of X-rays and neutrons can be particularly advantageous during an experiment to highlight structural or dynamic features of interest. In neutron scattering, the large difference in cross section between hydrogen and its isotope deuterium can be used to generate contrast between two phases that may otherwise be difficult to differentiate with microscopy techniques, such as two blended polymer phases demonstrated in our previous work.[64] The technique of tuning the SLD of materials in a complex sample to generate contrast is called contrast variation. Cao et al. implement contrast variation on dilute solutions of poly(3-decylthiophene) (P3DT) in an organic solvent to deconvolute the structure of the backbone and side chains in the molecule.[65] Without contrast manipulation, SANS would only provide information on chain rigidity for the whole molecule. However, it is specifically the backbone structure and fluctuations that are important in the context of charge transport mechanisms. Therefore, the researchers also investigated the SANS data for P3DT with a deuterated side chain (P3DT-d21) at varying ratios of hydrogenated and deuterated solvent, which highlighted either the backbone or side-chain structure. They find both with contrast variation SANS measurements and complementary coarse-grained MD simulations that the backbone has a lower rigidity when compared to the rigidity of the whole molecule as captured in SANS measurements of fully hydrogenated polymers, as shown in Figure 7. This overestimation of the chain rigidity would influence our understanding the of relationship between chain structure and charge transport mechanisms.

There are numerous examples showcasing the use of neutron scattering to characterize and understand molecular structure and dynamics of conjugated polymers. Bastianini et al. use SANS to follow the progression of P3HT from individual chains in solution to self-assembled nanofibers, which grow lengthwise in the $\pi$-stacking direction and provide favorable pathways for charge transport.[66] By fitting the SANS data to a combined Porod−Guinier model, they extract the Porod exponent, $m$, and the dimensionality factor, $s$, which provide information about the particle shapes. At high temperatures, the chains remain in globular form, suggesting that this is limiting the formation of nanofibers and maintaining a higher solubility. After the temperature is reduced, the chains begin to form elongated 1D structures, and after aging at this low temperature, 2D lamellae and nanofibers form in solution. These structures are then reversed during a final heating of the solution. This work demonstrates how SANS can be a powerful tool for *in situ* characterization of conjugated polymer self-assembly and can inform future tuning of these materials for improved performance. Guilbert et al. used a combined QENS and MD simulation approach to understand the effects of blending P3HT and PCBM, a relevant blend for OPV active layers, on the dynamics of the two molecules.[67] They note that the simulations were an essential component for achieving a thorough understanding of their experimental results, uncovering a wrapping of the P3HT chains around the PCBM molecules with the thiophene rings oriented cofacial to the PCBM. This structure was found to hinder side-chain dynamics of P3HT while enhancing those of PCBM side chains. The researchers point out that developing a thorough understanding of interactions between donor and acceptor molecules is important for understanding the influence of charge transport and phase morphology in these blends on overall device performance.

### B. Quantitative Comparison of Metrics from Scattering and Atomistic Molecular Dynamics Simulations

An advantage of using scattering as a validation tool for atomistic MD simulations is that they can be directly compared through the static structure factors (e.g., WAXS) or via the intermediate scattering functions (e.g., QENS). The static structure factor for any arbitrary distribution of atoms is calculated with the following formula[68,69]

$$S(q) = \frac{1}{\Sigma_{j=1}^{N_{species}} n_j Z_j^2}\Sigma_{\alpha,\beta\geq\alpha}^{N} Z_\alpha Z_\beta \langle e^{-i\vec{q}\cdot\vec{r}_\alpha} e^{-i\vec{q}\cdot\vec{r}_\beta}\rangle \tag{16}$$

where $N_{species}$ is the total number of atom types (i.e., isotopes), $N$ is the total number of atoms, $Z_\alpha$ and $Z_\beta$ are weight factors corresponding to the atomic numbers of atoms $\alpha$ and $\beta$ for the case of X-rays, $q$ is the scattering vector, and $r_\alpha$ and $r_\beta$ are the positions of atoms $\alpha$ and $\beta$. It is also possible to use the structure factor to compare with results from neutron diffraction, an approach employed by Alvarez, Arbe, Colmenero, Richter, and co-workers to study polystyrene, poly(alkylene oxide)s, polyisoprene, and many other classical polymers.[70−77] Although neutron diffraction requires deuterated materials or the use of neutron polarization analysis to deconvolute the incoherent and coherent contributions, it enables the study of partial structure factors of specific local structures that would not be possible with X-rays.

The intermediate scattering function can be calculated from MD simulations using the following equations[68,69]


https://doi.org/10.1021/acspolymersau.1c00027
ACS Polym. Au 2021, 1, 134−152

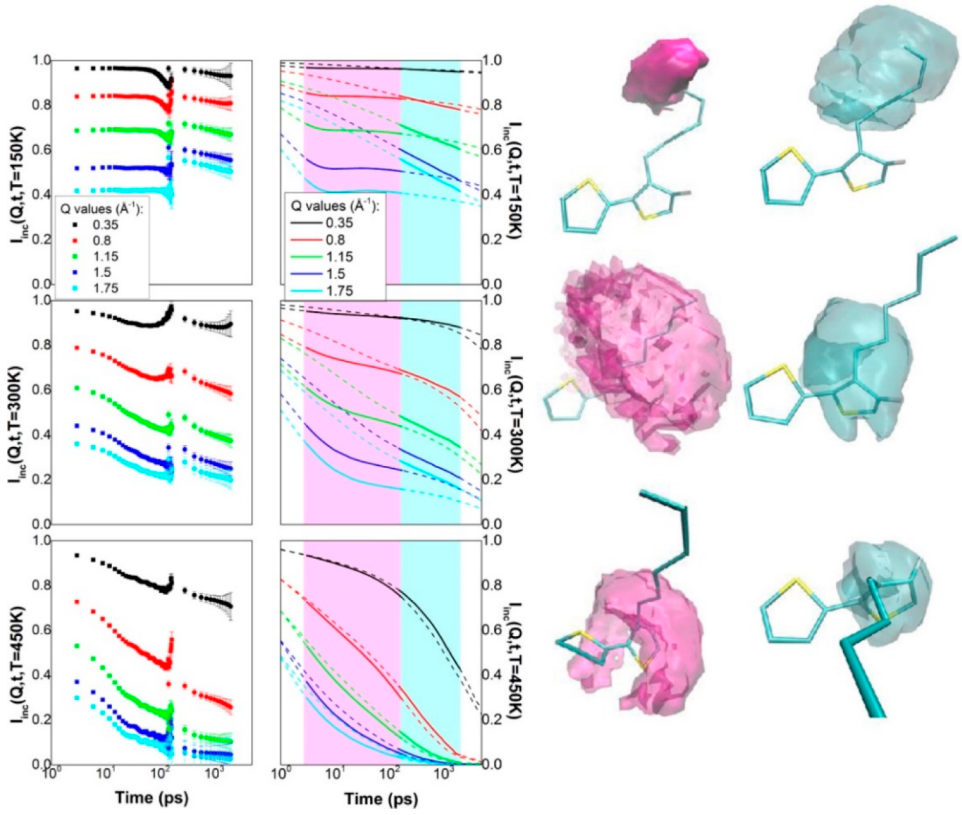


**Figure 8.** (Left) Intermediate scattering function extracted from QENS experiments for P3HT compared to (right) theoretical systems modeled using the Moreno et al. FF at three different temperatures that span below, approximately at, and above the glass-transition temperature. Colored areas correspond to the different subgroups of atoms and dynamics time scales of two different QENS instruments used in this work. Confidence intervals could not be shown for reprinted figures. Figure reprinted with permission from reference 88. Copyright 2015 American Chemical Society.

$$I_{inc}(q,\,t) = \frac{1}{\Sigma_{j=1}^{N_{species}} n_j b_{j,inc}^2} \Sigma_{\alpha=1}^{N} b_{\alpha,inc}^2 \langle e^{-i\vec{q}\cdot\vec{r_\alpha}(0)} e^{-i\vec{q}\cdot\vec{r_\alpha}(t)} \rangle \tag{17}$$

$$I_{coh}(q,\,t) = \frac{1}{\Sigma_{j=1}^{N_{species}} n_j b_{j,coh}^2} \Sigma_{\alpha,\beta\geq\alpha}^{N} b_{\alpha,coh} b_{\beta,coh} \langle e^{-i\vec{q}\cdot\vec{r_\alpha}(0)} e^{-i\vec{q}\cdot\vec{r_\beta}(t)} \rangle \tag{18}$$

$$I(q,\,t) = \frac{\Sigma_{j=1}^{N_{species}} n_j b_{j,inc}^2 I_{inc}(q,\,t) + \Sigma_{j=1}^{N_{species}} n_j b_{j,coh}^2 I_{coh}(q,\,t)}{\Sigma_{j=1}^{N_{species}} n_j b_{j,inc}^2 + \Sigma_{j=1}^{N_{species}} n_j b_{j,coh}^2} \tag{19}$$

where $N_{species}$ is the total number of atom types (i.e., isotopes), $n_j$ is the number of atoms of isotope $J$, $N$ is the total number of atoms, $b_{i,inc}$ and $b_{i,coh}$ are the incoherent and coherent scattering lengths of isotope $i$, $b_{\alpha,inc}$ and $b_{\alpha,coh}$ are the incoherent and coherent scattering lengths of atom $\alpha$, $q$ is the scattering vector, and $r_\alpha(t)$ and $r_\beta(t)$ are the positions of atoms $\alpha$ and $\beta$ at a time $t$. The mean squared displacement (MSD) can also be used to directly compare simulation results with those of QENS elastic scans. By selecting a time scale corresponding to the instrument's resolution, the MSD is calculated by

$$\text{MSD} = \left\langle \frac{1}{\Sigma_{\alpha=1}^{N}(\sigma_{\alpha,inc} + \sigma_{\alpha,coh})} \Sigma_{\alpha=1}^{N} (\sigma_{\alpha,inc} + \sigma_{\alpha,coh}) \cdot (\left\| \vec{r_\alpha}(\tau + \tau_O) - \vec{r_\alpha}(\tau_O) \right\|_F)^2 \right\rangle_\tau \tag{20}$$

where $N$ is the total number of atoms, $\sigma_{\alpha inc}$ and $\sigma_{\beta inc}$ are the incoherent and coherent scattering cross sections, $\vec{r_\alpha}(\tau_O)$ is the positional vector at time $\tau_O$, $\vec{r_\alpha}(\tau + \tau_O)$ is the positional vector at a time $\tau + \tau_O$ of atom $\alpha$, and $F$ is the Frobenius, or Euclidean, norm.

There are now several software tools available to calculate these and other relevant properties that enable direct comparison of atomistic MD simulation results to X-ray and neutron scattering experiments. nMoldyn[69,78,79] focuses on interfacing MD simulations with neutron scattering data and can calculate quantities including static and dynamic structure factors, coherent and incoherent intermediate scattering functions, mean squared displacement, and more. A related and more recent software, MDANSE, has a useful user-friendly interface and is actively supported by the Institut Laue-Langevin. LiquidLib[80] also focuses on quantitative analysis of MD simulation trajectories with neutron scattering for liquid systems. Overall, these packages are particularly useful for comparing simulations to experimental QENS measurements. We also note ATSAS,[81] a suite of software packages focused on analysis of small-angle scattering data. While there is a focus for use on biomacromolecules, the software is easily extendable to study a broader array of systems such as the solution conformation of CPs. Some specific programs to note include CRYSOL and CRYSON, which can generate SAXS and SANS profiles of macromolecules in solution from MD-derived molecular "snapshots". Sassena[82] takes a parallel computing approach to reduce the computational expense of calculating scattering profiles from massive MD simulations. Another software, SASSIE,[83] can be used to generate SANS or SAXS profiles from a generated conformation sampling of molecular


https://doi.org/10.1021/acspolymersau.1c00027
ACS Polym. Au 2021, 1, 134−152

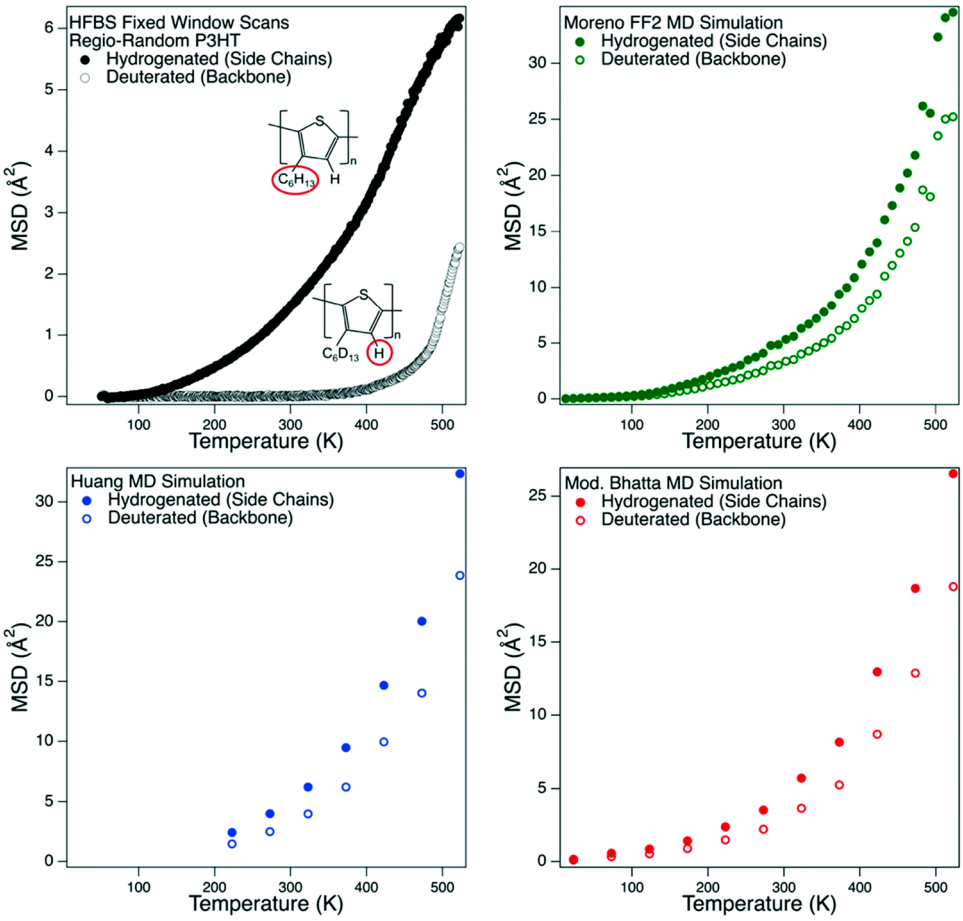


**Figure 9.** Mean squared displacement (MSD) of fully hydrogenated regiorandom P3HT and partially deuterated (along the side chain) regiorandom P3HT. Shown in the upper left is the experimental MSD extracted from QENS elastic scans. In the other panels are results from atomistic molecular dynamics simulations of regiorandom P3HT using the FF of Moreno et al.[23] (Moreno FF2), Bhatta et al.[40] (Mod. Bhatta FF), and Schwarz et al.[42,43] (Huang FF). Confidence intervals could not be shown for reprinted figures. Figure reprinted with permission from reference 20. Copyright 2019 The Royal Society of Chemistry.

structures and is particularly useful for exploring large conformation spaces of macromolecules that may not be achievable with MD. An advantage of many of these software packages is that they are open source and Python-based, making them widely accessible and compatible with Python-based high-throughput and machine learning (ML) packages.

### C. Quasielastic Neutron Scattering for Validation of Atomistic Force Fields

As previously mentioned, QENS has been an underutilized but powerful tool to combine with molecular modeling for a thorough study of CPs and for the quantitative validation of CP FFs for more physically accurate simulations. Arbe, Alvarez, and Colmenero also emphasize these points in reviews[61,84] advocating for the combined analysis of neutron scattering and simulations. The group has successfully applied this to uncover local structure and dynamics in classical polymers, including poly(ethylene oxide),[70] poly(vinyl acetate),[72] poly(methyl methacrylate),[85] and others.[71,73−77] Still, there are currently only a handful of works that implement a combined QENS and MD approach for CPs.[63,67,86−88] We introduced earlier the work of Guilbert et al., who used MD simulations to uncover interactions between P3HT and PCBM.[67,87] The researchers were also interested in using QENS to validate system dynamics that were generated by atomistic simulations of P3HT and poly(3-octylthiophene) (P3OT).[88] They found that the simulated and experimental approaches agreed well, which provided them with detailed *in silico* information into the picosecond to nanosecond dynamics that experiments could not provide alone. Figure 8 shows a comparison of the intermediate scattering function for P3HT that was extracted from QENS experiments and the results of MD simulations using the FF proposed by Moreno et al.[23] Through this quantitative comparison, they were also able to understand contributions from different subgroups of atoms within the two dynamic windows above and below the glass-transition temperature of the material.[88] More recently, the team used contrast variation in a collection of neutron scattering techniques in parallel with MD and ab initio simulations to provide a thorough characterization of the P3HT dynamics.[86] This allowed them to bridge structural features to self- and pair-correlated motions in the material. Finally, we note the work of Zhan et al. that demonstrated the influence of side-chain dynamics on backbone fluctuations in P3HT and P3DDT using combinations of MD simulations, QENS and SANS.[63] They found that longer side chains lead to enhanced dynamics and decreased rigidity of the conjugated backbone, which would directly influence any intrachain charge transport mechanisms.

In a previous work,[20] we also used QENS to compare the accuracy of five different FFs that had been proposed in the


https://doi.org/10.1021/acspolymersau.1c00027
ACS Polym. Au 2021, 1, 134−152

literature for P3HT in works by Moreno et al.,[23] Bhatta et al.,[40] and Schwarz et al.[42,43] As previously discussed, all of these used a classical FF that was modified with reparametrized atomic partial charges and dihedral potentials along the chain backbone to account for the effects of conjugation. Simulations of regiorandom P3HT using these FFs resulted in differing *in silico* structure and dynamics, including differences in the distribution of *cis*- and *trans*-conformations between monomers along the chain, the degree of twisting between monomers, and radial distribution of thiophene−thiophene distances in the material. Conjugation along the polymer backbone and $\pi$-orbital overlap of neighboring chains are very sensitive to these parameters, and charge transport simulations performed on frames obtained from these simulations would be greatly influenced by the specific choice of FF. When comparing the modeled systems to QENS results, we find that all FFs captured the overall system dynamics reasonably well when the polymers where fully hydrogenated and the side-chain motions dominated the signals. However, when alkyl side chains were deuterated to increase sensitivity toward the P3HT backbone, a significant limitation of all investigated FFs was uncovered. Figure 9 shows the mean squared displacement (MSD) that is extracted from QENS fixed window scans for fully hydrogenated and partially deuterated P3HT. Due to the significantly larger incoherent cross section of hydrogen, dynamics of the alkyl side chains is the primary contributor to the dynamics in the fully hydrogenated material, while sensitivity toward backbone motions is maximized in the partially deuterated material. We find that dynamic motions of the side chains begin at very low temperatures (<200 K), while the dynamics of the backbone has a significantly delayed relaxation and only become significant at temperatures above 400 K. For comparison, Figure 9 shows MSDs calculated from three of the modeled systems. Qualitatively, all FFs capture the dynamics of the alkyl side chains reasonably well but fail to capture the delayed relaxation of the backbone. By utilizing QENS and partial deuteration, it was possible to quantify the capabilities and limitation of these FFs at time scales ranging between picoseconds and nanoseconds. This highlights how neutron scattering, when coupled with contrast variation, can provide a very large and rigorous data set that could be subsequently used for testing, benchmarking, and continuous improvement of future FFs for CP systems. Given the considerable expense of synthesizing good quality CPs with partial deuteration as well as the expense associated with performing neutron scattering experiments, it is imperative that such data sets are openly available and documented for their future use.

## IV. REPARAMETERIZATION OF NONBONDED PARAMETERS IN CONJUGATED POLYMER FORCE FIELDS

In current reparametrized FFs for CPs, the parameters expected to be most significantly affected by conjugation include partial charges and inter-ring torsion potentials. Past work demonstrates that reparametrized FFs can capture structural properties of CPs very well but also that they fail to capture characteristic backbone dynamics that would directly influence charge transport. This does not suggest that dihedral potentials and partial charges are unimportant but rather that we need to take a critical look at other components of the FF that may also be affected by conjugation.

Intermolecular forces in condensed phases involve complex Coulombic, polar, and induced polarization interactions that have been described in great depth in several texts. The reader is referred to the work by Israelachvili[89] for a thorough introduction. Since these physically inspired parameters are all highly sensitive to the electronic orbitals of the atoms that make up these macromolecules, it is logical to anticipate that conjugation and electronic delocalization should significantly affect their values. However, as shown in Table 1, few works have attempted to reparametrize these nonbonded components in FFs for CPs. Marcon and co-workers mention that stronger dispersion forces would be found in conjugated polymers due to the increased polarizability caused by the electron delocalization along the chain.[34] Davies et al. found a theoretical power law dependence of polarizability on the molecular weight of polyacetylene, again due to the long-range electron deleocalization.[90] Schmit and Levine also studied polyacetylene and found that, as two chains approached each other in a cross formation, an additional strong binding force presented itself due to electron tunneling between the chains.[91] This electron delocalization is critical to the electronic performance of CPs. We can consider the importance of exciton movement through donor and acceptor phases of an OPV active later to reach the respective cathode and anode surfaces. Marchiori et al. found that the orientation of induced dipoles can influence the exciton dissociation at the P3HT and PCBM interface and that this behavior would be influenced by long-range polarization.[92] Overall, $\pi$-conjugation in CPs results in increased polarizability that would modify the van der Waals forces. Although MD simulations cannot capture these quantum-mechanical effects, it is important that intermolecular interactions are represented as accurately as possible within the classical FF definition to adequately represent realistic structures and dynamics for CPs.

While we point out that most reparametrized FFs for CPs do not update the nonbonded Lennard-Jones interactions, a few have made some modifications of classical models. DuBay et al. employed a buffered 14/7 functional form rather than the more common 12/6 Lennard-Jones form to reduce the electrostatic repulsive forces.[39] Marcon and co-workers employed a Buckingham potential with modified parameters for the carbon atoms that resulted in an attractive well depth that was 39% deeper relative to the depth generated by the classical Lennard-Jones MM3[31−33] parameters to account for the underestimated density of oligothiophenes.[34] In another work focused on oligofluorenes, the authors again found that the attractive component to the Buckingham potential needed to be even stronger to account for the underestimated density.[36]

To further investigate the effects of conjugation in the nonbonded interactions, we extracted partial charges and Lennard-Jones parameters from the FF of Moreno et al.[23] and calculated the total combined nonbonded interaction energy between two P3HT oligomers of various lengths. This model, as well as most of the FFs reviewed in Section II, borrow the classical nonbonded parameters. However, these parameters are frequently determined from empirical fits of small molecules. For FFs utilizing a base of OPLS-AA, these parameters are taken from those of molecular thiophene or benzene. Figure S1 of the Supporting Information shows the Coulombic and Lennard-Jones contributions to the nonbonded interaction energies determined from the FF of Moreno et al.[23] The results show that the Lennard-Jones


https://doi.org/10.1021/acspolymersau.1c00027
ACS Polym. Au 2021, 1, 134−152

interactions, rather than the Coulombic terms that are modulated by the partial charges, make the most significant contribution to the net interaction energy, which also supports our past findings[20] demonstrating that modifying partial charges across FFs did not significantly improve agreement between experimental and simulated dynamics of regiorandom P3HT. Furthermore, when the net interaction energy is normalized by the chain length, after a chain length of six monomers (hexamer), the attraction between molecules (depth of the well) converges. Nonbonded potential energies from published CP FFs can also be further compared to DFT computations performed on P3HT oligomers at the B3LYP/6-311++g** level of theory to determine if the impact of conjugation could be significant. A thorough methods section for these DFT calculations is provided in the Supporting Information. Figure 10 shows that, unlike the potential energy

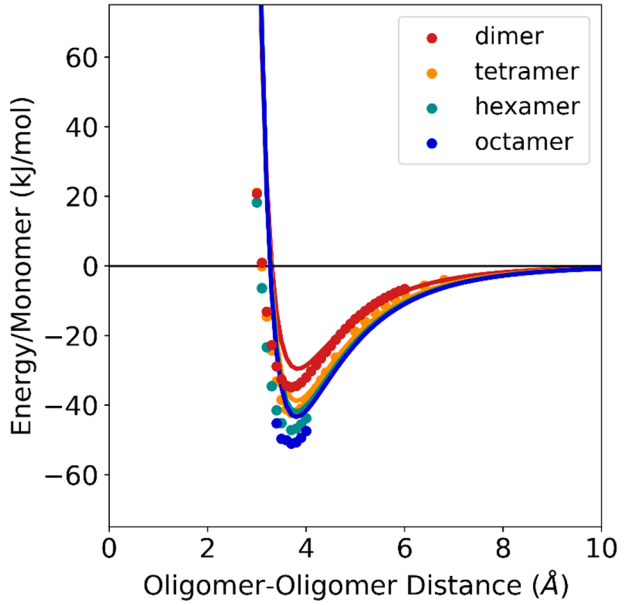


**Figure 10.** Nonbonded interactions determined by ab initio calculations at the B3LYP/6-311++g(d,p) level of theory with D3 dispersion corrections (markers) compared to those determined by the Lennard-Jones potential parametrized in Moreno et al.[23] FFs (lines) between two P3HT oligomers.

from MD FFs, the normalized nonbonded interaction energy from DFT does not converge. Instead, it continues to diverge from the "classical" approximation of the Moreno et al.[23] FF. These results suggest that the Moreno FF is likely underestimating the nonbonded interaction strength, most considerably as the molecular weight of P3HT increases, where the conjugation length could be significant.

We note, however, that the strength of these interactions has been shown to be highly sensitive to the level of theory at which the ab initio calculations are performed,[93] adding to the complexity and challenge of parametrizing accurate nonbonded interaction parameters for CP FFs. Another limitation of this approach is the high computational expense of performing ab initio calculations. We emphasize that the point of these calculations is not to provide quantitative replacements for Lennard-Jones potentials in MD simulations but rather to demonstrate the need to also reparametrize nonbonded Lennard-Jones interactions. Atomistic MD FFs aim to capture complex quantum-mechanical interactions within a simple and computationally efficient functional. Ultimately, the aim is to obtain a meaningful representation of the physical system to further interrogate it via computations. Still, traditional parametrization approaches require a complex, synergistic, and hierarchical approach to building up the full parameter set. The approach of isolating specific interactions, such as dihedral potentials between monomers along CP backbones or the partial charges, for reparameterization via ab initio calculations has been necessary to manage the significant computational expense that is associated with full FF development. This is especially complex when considering that, for CPs, this process needs to be repeated for each new molecule of interest due to the complex variation in electronic energy levels that is possible to achieve. Fortunately, this expensive approach toward FF parametrization has already begun to shift with the introduction of powerful new methods in computational chemistry, machine learning, and data science. When combined with the rich and expansive data that can originate from neutron scattering experiments, these methods promise a bright future for the *in silico* design of advanced conjugated soft materials.

## V. OPPORTUNITIES FOR HIGH-THROUGHPUT FORCE FIELD DEVELOPMENT

Including Lennard-Jones parameters in the reparameterization process for CP FFs offers an opportunity for improving the accuracy of MD simulations, such as adequately capturing the backbone dynamics that is relevant to important charge transport mechanisms. However, the use of current reparameterization procedures is already not sustainable given the large computational expense and the rapidly increasing diversity of CP molecules that become available. For almost two decades, researchers have been exploring a range of parametrization methods and validation metrics in pursuit of physically accurate CP FFs, but existing models still fail to capture accurate dynamics in the simplest of model systems (e.g., polythiophenes). If we hope to ever enable the use of MD simulations to predict and design the performance of advanced CPs for new technologies, we need a new robust, accurate, and efficient process for FF parametrization. Advances in computational hardware and software have decreased computation time, but these are still insufficient to overcome the arduous process of FF parametrization. We propose to consider the use of automated and higher-level ML approaches, as well as the implementation of oligomers as proxies for longer polymer chains, to realize a high-throughput approach to a more accurate experimentally validated FF parametrization.

Researchers have already begun applying ML approaches to FF development across a broad range of materials and applications. For example, Botu et al. developed an AGNI FF, the name of which pointed out the adaptive, generalizable, and neighborhood informed qualities of their model.[94,95] Their training set included DFT and ab initio MD simulations of local atomic environments, including within bulk phases, at surfaces, and near defects, in elemental materials and the resulting forces felt by the atoms. They created a fingerprint to map local atomic environments to resulting forces and trained a nonlinear kernel ridge regression method to predict the force at each step within the MD simulation. The team notes that while their approach can be easily applied to multielement materials, the model becomes exponentially more complex to develop as the material's complexity increases. Nevertheless,


https://doi.org/10.1021/acspolymersau.1c00027
ACS Polym. Au 2021, 1, 134−152

their models enabled accurate and computationally inexpensive MD simulations. The approach of Jinnouchi et al. is similar, but the team uses a Bayesian linear-regression model to only perform ab initio calculations of local atomic environments when needed, i.e., when a new local environment is encountered during a simulation.[96] The model is then updated with the new information to determine the FF parameters and their derivatives to update each atom's position and velocity accordingly. For a more in-depth review of these types of ab initio ML FFs, we refer the reader to a recent review by Unke et al.[97] Their work not only provides a thorough review of the fundamentals behind the ML models used and how these types of FFs can be generated, but the authors also carefully note the advantages and limitations of this approach. One of the discussed limitations for these ab-initio-based models is that they remain computationally expensive compared to classical FFs and MD simulations. Another recent work by Befort et al. describes an alternative top-down approach to ML-parametrized FFs.[98] Their workflow incorporates experimental validation, domain knowledge, and surrogate models to perform an extensive optimization of Lennard-Jones parameters for two different small molecules with an objective to reproduce either the vapor−liquid equilibrium or crystal structure. The authors also note that with such an exhaustive exploration of the parameter search space, they can better understand whether a model is limited by the optimized parameters, the unoptimized parameters, or the chosen functional form of the FF.

With a similar top-down ML approach, we propose that the use of ML approaches to perform on-the-fly MD simulations of CPs could capture larger-scale dynamics that are not accessible with *ab initio* methods and fit classical MD FF parameters to reproduce the structure and dynamics that are captured by neutron and X-ray scattering experiments. Bayesian (and other) ML approaches would improve the automation of FF parametrization and would also be able to cover a broader search space of relevant parameters than what researchers could reasonably do with current approaches. We recognize that a significant rate-limiting step in this approach is the computational expense of the MD simulations that are used for generating scattering profiles. Even if we employ parallel computing approaches, large-scale simulations of full-size CPs can require days or weeks to complete. Therefore, we also propose that researchers should consider the use of oligomers as proxies for longer CPs to reduce the time required to perform the requisite MD simulations. While it is known that the electronic and mechanical behavior of CPs is sensitive to molecular weight, it has been demonstrated that local molecular fluctuations, e.g., dihedral twisting along the backbone, converge to those of longer chains at a moderate length. The work of Bhatta et al. explored the dynamics of P3HT dynamics at varying oligomer lengths and found that, after a chain length of 10−12 monomers, oligomers demonstrated behaviors representative of polymeric equivalents.[57] Moreover, our previous work has demonstrated that the existing MD FFs for CPs fail to capture these local dynamics, even for a simple molecule like P3HT, and that these local motions are directly tied to charge transport mechanisms.[20] We propose the use of oligomers for a high-throughput development of accurate, experimentally validated CP FFs. The use of oligomers as a substitute will reduce the computational expense of the MD simulations (on the order of atom count[99]) while still capturing the localized dynamics relevant to charge transport and, if the oligomer length is sufficiently long as previously discussed, that is representative of those in longer chains. While future simulations utilizing the optimized force field should implement full chains representative of the material's molecular weight, the use of oligomers during the FF optimization can enable this powerful approach for more accurate models.

As a starting place for the proposed approach, we also collected QENS data for partially deuterated and fully hydrogenated forms of regioregular (semicrystalline) P3HT polymers and oligomers and provide it openly for use in validation by researchers interested in FF development. Figure 11 shows mean squared displacement results for QENS elastic scans. The intermediate scattering functions for the same samples are also provided in the Supporting Information as a compressed data file. For the P3HT polymers, the side chains begin to relax at low temperatures below 200 K, while the backbone dynamics relax after 440 K, similar to the results presented in Figure 9 for regiorandom (amorphous) P3HT. Moreover, the transition point for RRe-P3HT-D13 aligns at the melting point of the material at approximately 475 K. However, for the P3HT oligomers, the difference between the side-chain and backbone dynamics is more subtle, and we hypothesize that this is due to a lower-temperature relaxation of the backbone in shorter chains. Overall, this data provides opportunities for a thorough investigation into origin of these phase transitions using MD simulations. In the Supporting Information, we provide the full data sets to encourage open science and broad utilization by the community. While neutron scattering provides a powerful tool to uncovering dynamics along the backbone and side-chain regimes of CPs, synthesizing selectively deuterated molecules and collecting neutron scattering data is not always readily achievable. However, utilizing data collected broadly by the community can help us in pursuit of implementing ML approaches for accurate CP

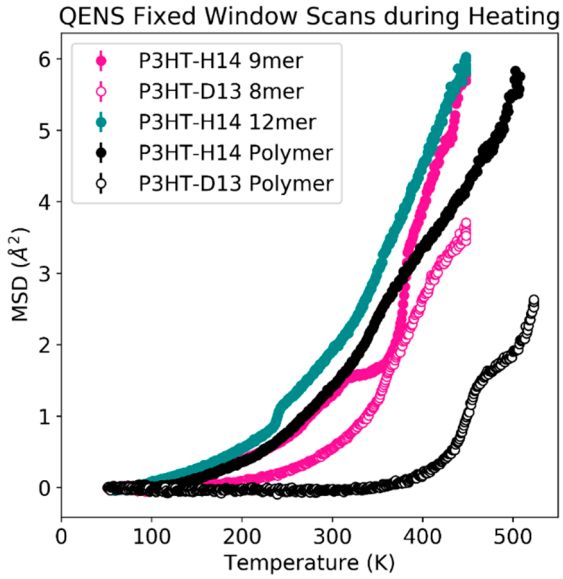


**Figure 11.** Fixed window scans (elastic scans) collecting during warming on the High Flux Backscattering Spectrometer (HFBS) at the NIST Center for Neutron Research for hydrogenated and partially deuterated regioregular poly(3-hexylthiophene) (RRe-P3HT) polymers and oligomers. Error bars representing standard deviations are provided but are smaller than the marker sizes and not visible.


https://doi.org/10.1021/acspolymersau.1c00027
ACS Polym. Au 2021, 1, 134−152

FFs. Broad and open collaboration between experimentalists and computational researchers will be critical and essential to advancing the computational accuracy of simulations aiming to describe complex electronically conjugated materials.

## VI. CONCLUSION

In this work, we have reviewed the powerful nature of a combined MD, X-ray, and neutron scattering approach to achieve deep understanding in the relationship between the molecular structure and dynamics, charge transport mechanisms, and macroscopic electronic performance in CPs. These computational models require the use of accurate FFs, yet the existing reparametrized CP FFs still fail to capture backbone dynamics relevant to charge transport mechanisms in a very simple model system of polythiophene after almost two decades of effort. Moreover, we find that the current reparameterizations exclude critical force field parameters such as the Lennard-Jones potential, which are significantly affected by the large-scale conjugation along the polymer chains. However, broadening the parametrization space for more accurate CP FFs will not be sustainable with current parametrization approaches. Therefore, we propose the use of ML, such as Bayesian methods, to automate this process and generate empirically fit FF parameter sets for new CPs using neutron and X-ray scattering data sets that capture structure and dynamics at commensurate length and time scales. This will open a broader computational space to explore structure–function relationships in CPs and tune new molecules for improved efficiencies and to enable new technologies.

## ■ ASSOCIATED CONTENT

### Supporting Information

The Supporting Information is available free of charge at https://pubs.acs.org/doi/10.1021/acspolymersau.1c00027.

Additional methods for density functional theory calculations, synthesis and characterization of P3HT oligomers and polymers, and experimental details for quasielastic neutron scattering measurements (PDF)

Compressed file including reduced quasielastic neutron scattering data for P3HT oligomers and polymers (ZIP)

## ■ AUTHOR INFORMATION


### Corresponding Authors

**Caitlyn M. Wolf** − *Department of Chemical Engineering, University of Washington, Seattle, Washington 98195-1750, United States; Center for Neutron Research, Stop 6102, National Institute of Standards and Technology, Gaithersburg, Maryland 20889-6102, United States;* orcid.org/0000-0002-2956-7049; Email: caitlyn.wolf@nist.gov

**Lilo D. Pozzo** − *Department of Chemical Engineering, University of Washington, Seattle, Washington 98195-1750, United States;* orcid.org/0000-0001-7104-9061; Email: dpozzo@uw.edu

### Authors

**Lorenzo Guio** − *Department of Material Science and Engineering, University of Washington, Seattle, Washington 98195-2120, United States*

**Sage Scheiwiller** − *Department of Chemical Engineering, University of Washington, Seattle, Washington 98195-1750, United States;* orcid.org/0000-0003-2362-7933

**Viktoria Pakhnyuk** − *Department of Chemistry, University of Washington, Seattle, Washington 98195-1700, United States*

**Christine Luscombe** − *Department of Material Science and Engineering, University of Washington, Seattle, Washington 98195-2120, United States; Department of Chemistry, University of Washington, Seattle, Washington 98195-1700, United States;* orcid.org/0000-0001-7456-1343

Complete contact information is available at: https://pubs.acs.org/10.1021/acspolymersau.1c00027


### Notes

The authors declare no competing financial interest.

## ■ ACKNOWLEDGMENTS

Primary support for this work was provided by the Department of Energy Office of Basic Energy Sciences under award number DE-SC0019911. Caitlyn Wolf was also supported by an NSF IGERT DGE-1258485 fellowship and through the University of Washington Clean Energy Institute, which provided access to facilities for testing and preparation of samples. Viktoria Pakhnyuk and Christine K. Luscombe also thank NSF DMR-2104234 for support. This work was facilitated through the advanced computational, storage, and networking infrastructure provided by the Hyak supercomputer system, which is partially funded by the student technology fee (STF) at the University of Washington. We also acknowledge the support of the National Institute of Standards and Technology (NIST), U.S. Department of Commerce, in providing the neutron research facilities located at the NIST Center for Neutron Research (NCNR) used in this work. Access to the High Flux Backscattering Spectrometer (HFBS) and Neutron Spin Echo (NSE) Spectrometer was provided by the Center for High Resolution Neutron Scattering (CHRNS), a partnership between the National Institute of Standards and Technology and the National Science Foundation under Agreement No. DMR-1508249. Certain commercial material suppliers are identified in this paper to foster understanding. Such identification does not imply recommendation or endorsement by the National Institute of Standards and Technology nor does it imply that the materials or equipment identified are necessarily the best available for this purpose. This work also used resources (BASIS) at the Spallation Neutron Source (SNS), a DOE Office of Science User Facility operated by the Oak Ridge National Laboratory. A portion of material synthesis was also supported by the Center for Nanophase Materials Sciences, which is a DOE Office of Science User Facility. Finally, we thank Madhusudan Tyagi and Antonio Faraone at the NCNR and Naresh Osti at the SNS for their contributions during the neutron experiments.

## ■ LIST OF ABBREVIATIONS

| | |
|---|---|
| AMBER | Assisted Model Building with Energy Refinement force field |
| CHARMM | Chemistry at Harvard Macromolecular Mechanics force field |
| CP | conjugated polymer |
| DFT | density functional theory |
| FF | force field |

| | |
|---|---|
| GAFF | Generalized Assisted Model Building with Energy Refinement Force Field |
| GROMOS | Groningen Molecular Simulation force field |
| MD | molecular dynamics |
| ML | machine learning |
| MM3 | molecular mechanics force field |
| MSD | mean squared displacement |
| OPLS-AA | Optimized Potentials for Liquid Simulations All-Atom force field |
| OPV | organic photovoltaic |
| OLED | organic light-emitting diode |
| OFET | organic field-effect transistor |
| PBTTT | poly(2,5-bis(3-alkylthiophen-2-yl)thieno[2,3-*b*]-thiophene) |
| PEDOT | poly(3,4-ethyl-enedioxythiophene) |
| P3DDT | poly(3-dodecylthoiphene) |
| P3DT | poly(3-decylthiophene) |
| P3EHT | poly(3-(2′-ethyl)hexylthiophene) |
| P3HT | poly(3-hexylthiophene) |
| P3OT | poly(3-octylthiophene) |
| QENS | quasielastic neutron scattering |
| SANS | small-angle neutron scattering |
| SAXS | small-angle X-ray scattering |
| SLD | scattering length density |
| WAXS | wide-angle X-ray scattering |

## REFERENCES


(1) Sekine, C.; Tsubata, Y.; Yamada, T.; Kitano, M.; Doi, S. Recent Progress of High Performance Polymer OLED and OPV Materials for Organic Printed Electronics. *Sci. Technol. Adv. Mater.* **2014**, *15* (3), 034203.

(2) Li, Z.; Chueh, C.-C.; Jen, A. K.-Y. Recent Advances in Molecular Design of Functional Conjugated Polymers for High-Performance Polymer Solar Cells. *Prog. Polym. Sci.* **2019**, *99*, 101175.

(3) Mazzio, K. A.; Luscombe, C. K. The Future of Organic Photovoltaics. *Chem. Soc. Rev.* **2015**, *44* (1), 78.

(4) Sirringhaus, H. 25th Anniversary Article: Organic Field-Effect Transistors: The Path Beyond Amorphous Silicon. *Adv. Mater.* **2014**, *26* (9), 1319.

(5) Pandey, M.; Kumari, N.; Nagamatsu, S.; Pandey, S. S. Recent Advances in the Orientation of Conjugated Polymers for Organic Field-Effect Transistors. *J. Mater. Chem. C* **2019**, *7* (43), 13323.

(6) Alvarez, A.; Costa-Fernández, J. M.; Pereiro, R.; Sanz-Medel, A.; Salinas-Castillo, A. Fluorescent Conjugated Polymers for Chemical and Biochemical Sensing. *TrAC, Trends Anal. Chem.* **2011**, *30* (9), 1513.

(7) Huynh, T.-P.; Sharma, P. S.; Sosnowska, M.; D'Souza, F.; Kutner, W. Functionalized Polythiophenes: Recognition Materials for Chemosensors and Biosensors of Superior Sensitivity, Selectivity, and Detectability. *Prog. Polym. Sci.* **2015**, *47*, 1.

(8) Wang, M.; Baek, P.; Akbarinejad, A.; Barker, D.; Travas-Sejdic, J. Conjugated Polymers and Composites for Stretchable Organic Electronics. *J. Mater. Chem. C* **2019**, *7* (19), 5534.

(9) Fidanovski, K.; Mawad, D. Conjugated Polymers in Bioelectronics: Addressing the Interface Challenge. *Adv. Healthcare Mater.* **2019**, *8* (10), 1900053.

(10) Anantha-Iyengar, G.; Shanmugasundaram, K.; Nallal, M.; Lee, K.-P.; Whitcombe, M. J.; Lakshmi, D.; Sai-Anand, G. Functionalized Conjugated Polymers for Sensing and Molecular Imprinting Applications. *Prog. Polym. Sci.* **2019**, *88*, 1.

(11) Someya, T.; Bao, Z.; Malliaras, G. G. The Rise of Plastic Bioelectronics. *Nature* **2016**, *540* (7633), 379.

(12) Liao, C.; Zhang, M.; Yao, M. Y.; Hua, T.; Li, L.; Yan, F. Flexible Organic Electronics in Biology: Materials and Devices. *Adv. Mater.* **2015**, *27* (46), 7493.

(13) Lan, Y.-K.; Huang, C.-I. Charge Mobility and Transport Behavior in the Ordered and Disordered States of the Regioregular Poly(3-Hexylthiophene). *J. Phys. Chem. B* **2009**, *113* (44), 14555.

(14) Gu, K.; Snyder, C. R.; Onorato, J.; Luscombe, C. K.; Bosse, A. W.; Loo, Y.-L. Assessing the Huang-Brown Description of Tie Chains for Charge Transport in Conjugated Polymers. *ACS Macro Lett.* **2018**, *7* (11), 1333.

(15) Holliday, S.; Li, Y.; Luscombe, C. K. Recent Advances in High Performance Donor-Acceptor Polymers for Organic Photovoltaics. *Prog. Polym. Sci.* **2017**, *70*, 34.

(16) Kim, M.; Ryu, S. U.; Park, S. A.; Choi, K.; Kim, T.; Chung, D.; Park, T. Donor-Acceptor-Conjugated Polymer for High-Performance Organic Field-Effect Transistors: A Progress Report. *Adv. Funct. Mater.* **2020**, *30* (20), 1904545.

(17) McMahon, D. P.; Cheung, D. L.; Goris, L.; Dacuña, J.; Salleo, A.; Troisi, A. Relation between Microstructure and Charge Transport in Polymers of Different Regioregularity. *J. Phys. Chem. C* **2011**, *115* (39), 19386.

(18) Alberga, D.; Perrier, A.; Ciofini, I.; Mangiatordi, G. F.; Lattanzi, G.; Adamo, C. Morphological and Charge Transport Properties of Amorphous and Crystalline P3HT and PBTTT: Insights from Theory. *Phys. Chem. Chem. Phys.* **2015**, *17* (28), 18742.

(19) Tapping, P. C.; Clafton, S. N.; Schwarz, K. N.; Kee, T. W.; Huang, D. M. Molecular-Level Details of Morphology-Dependent Exciton Migration in Poly(3-Hexylthiophene) Nanostructures. *J. Phys. Chem. C* **2015**, *119* (13), 7047.

(20) Wolf, C. M.; Kanekal, K. H.; Yimer, Y. Y.; Tyagi, M.; Omar-Diallo, S.; Pakhnyuk, V.; Luscombe, C. K.; Pfaendtner, J.; Pozzo, L. D. Assessment of Molecular Dynamics Simulations for Amorphous Poly(3-Hexylthiophene) Using Neutron and X-Ray Scattering Experiments. *Soft Matter* **2019**, *15* (25), 5067.

(21) González, M. A. Force Fields and Molecular Dynamics Simulations. *École thématique de la Société Française de la Neutronique* **2011**, *12*, 169.

(22) Allen, M. P. Introduction to Molecular Dynamics Simulation. In *Computational Soft Matter: From Synthetic Polymers to Proteins, Lecture Notes*; Attig, N., Binder, K., Grubmüller, H., Kremer, K., Eds.; John von Neumann Institute for Computing: Jülich, 2004; Vol. *23*, pp 1−28.

(23) Moreno, M.; Casalegno, M.; Raos, G.; Meille, S. v.; Po, R. Molecular Modeling of Crystalline Alkylthiophene Oligomers and Polymers. *J. Phys. Chem. B* **2010**, *114* (4), 1591.

(24) Jorgensen, W. L.; Maxwell, D. S.; Tirado-Rives, J. Development and Testing of the OPLS All-Atom Force Field on Conformational Energetics and Properties of Organic Liquids. *J. Am. Chem. Soc.* **1996**, *118* (45), 11225.

(25) Jorgensen, W. L.; Tirado-Rives, J. Potential Energy Functions for Atomic-Level Simulations of Water and Organic and Biomolecular Systems. *Proc. Natl. Acad. Sci. U. S. A.* **2005**, *102* (19), 6665.

(26) Maxwell, D. S.; Tirado-Rives, J.; Jorgensen, W. L. A Comprehensive Study of the Rotational Energy Profiles of Organic Systems Byab Initio MO Theory, Forming a Basis for Peptide Torsional Parameters. *J. Comput. Chem.* **1995**, *16* (8), 984.

(27) Wang, J.; Wolf, R. M.; Caldwell, J. W.; Kollman, P. A.; Case, D. A. Development and Testing of a General Amber Force Field. *J. Comput. Chem.* **2004**, *25* (9), 1157.

(28) Klauda, J. B.; Venable, R. M.; Freites, J. A.; O'Connor, J. W.; Tobias, D. J.; Mondragon-Ramirez, C.; Vorobyov, I.; MacKerell, A. D.; Pastor, R. W. Update of the CHARMM All-Atom Additive Force Field for Lipids: Validation on Six Lipid Types. *J. Phys. Chem. B* **2010**, *114* (23), 7830.

(29) Scott, W. R. P.; Hünenberger, P. H.; Tironi, I. G.; Mark, A. E.; Billeter, S. R.; Fennen, J.; Torda, A. E.; Huber, T.; Krüger, P.; van Gunsteren, W. F. The GROMOS Biomolecular Simulation Program Package. *J. Phys. Chem. A* **1999**, *103* (19), 3596.

(30) Schmid, N.; Eichenberger, A. P.; Choutko, A.; Riniker, S.; Winger, M.; Mark, A. E.; van Gunsteren, W. F. Definition and Testing of the GROMOS Force-Field Versions 54A7 and 54B7. *Eur. Biophys. J.* **2011**, *40* (7), 843.




https://doi.org/10.1021/acspolymersau.1c00027
*ACS Polym. Au* 2021, 1, 134−152

(31) Allinger, N. L.; Yuh, Y. H.; Lii, J. H. Molecular Mechanics. The MM3 Force Field for Hydrocarbons. 1. *J. Am. Chem. Soc.* **1989**, *111* (23), 8551.
(32) Yang, L.; Allinger, N. L. MM3 Calculations of Aromatic Heterocyclic Compounds: Sulfur-Nitrogen Containing Molecules. *J. Mol. Struct.: THEOCHEM* **1996**, *370* (1), 71.
(33) Lii, J. H.; Allinger, N. L. Molecular Mechanics. The MM3 Force Field for Hydrocarbons. 2. Vibrational Frequencies and Thermodynamics. *J. Am. Chem. Soc.* **1989**, *111* (23), 8566.
(34) Marcon, V.; Raos, G. Molecular Modeling of Crystalline Oligothiophenes: Testing and Development of Improved Force Fields. *J. Phys. Chem. B* **2004**, *108* (46), 18053.
(35) Marcon, V.; Raos, G. Free Energies of Molecular Crystal Surfaces by Computer Simulation: Application to Tetrathiophene. *J. Am. Chem. Soc.* **2006**, *128* (5), 1408.
(36) Marcon, V.; van der Vegt, N.; Wegner, G.; Raos, G. Modeling of Molecular Packing and Conformation in Oligofluorenes. *J. Phys. Chem. B* **2006**, *110* (11), 5253.
(37) Widge, A. S.; Matsuoka, Y.; Kurnikova, M. Development and Initial Testing of an Empirical Forcefield for Simulation of Poly(Alkylthiophenes). *J. Mol. Graphics Modell.* **2008**, *27* (1), 34.
(38) Allen, F. H. The Cambridge Structural Database: A Quarter of a Million Crystal Structures and Rising. *Acta Crystallogr., Sect. B: Struct. Sci.* **2002**, *58* (3), 380.
(39) DuBay, K. H.; Hall, M. L.; Hughes, T. F.; Wu, C.; Reichman, D. R.; Friesner, R. A. Accurate Force Field Development for Modeling Conjugated Polymers. *J. Chem. Theory Comput.* **2012**, *8* (11), 4556.
(40) Bhatta, R. S.; Yimer, Y. Y.; Perry, D. S.; Tsige, M. Improved Force Field for Molecular Modeling of Poly(3-Hexylthiophene). *J. Phys. Chem. B* **2013**, *117* (34), 10035.
(41) Łużny, W.; Piwowarczyk, K. Molecular Dynamics Simulations of Poly(Alkylthiophenes): An Overall View of Some Recent Results. *Synth. Met.* **2013**, *179*, 1.
(42) Schwarz, K. N.; Kee, T. W.; Huang, D. M. Coarse-Grained Simulations of the Solution-Phase Self-Assembly of Poly(3-Hexylthiophene) Nanostructures. *Nanoscale* **2013**, *5* (5), 2017.
(43) Huang, D. M.; Faller, R.; Do, K.; Moulé, A. J. Coarse-Grained Computer Simulations of Polymer/Fullerene Bulk Heterojunctions for Organic Photovoltaic Applications. *J. Chem. Theory Comput.* **2010**, *6* (2), 526.
(44) Jackson, N. E.; Kohlstedt, K. L.; Savoie, B. M.; Olvera de la Cruz, M.; Schatz, G. C.; Chen, L. X.; Ratner, M. A. Conformational Order in Aggregates of Conjugated Polymers. *J. Am. Chem. Soc.* **2015**, *137* (19), 6254.
(45) Wildman, J.; Repiščák, P.; Paterson, M. J.; Galbraith, I. General Force-Field Parametrization Scheme for Molecular Dynamics Simulations of Conjugated Materials in Solution. *J. Chem. Theory Comput.* **2016**, *12* (8), 3813.
(46) Kaminski, G. A.; Friesner, R. A.; Tirado-Rives, J.; Jorgensen, W. L. Evaluation and Reparametrization of the OPLS-AA Force Field for Proteins via Comparison with Accurate Quantum Chemical Calculations on Peptides †. *J. Phys. Chem. B* **2001**, *105* (28), 6474.
(47) Price, M. L. P.; Ostrovsky, D.; Jorgensen, W. L. Gas-Phase and Liquid-State Properties of Esters, Nitriles, and Nitro Compounds with the OPLS-AA Force Field. *J. Comput. Chem.* **2001**, *22* (13), 1340.
(48) Jorgensen, W. L.; McDonald, N. A. Development of an All-Atom Force Field for Heterocycles. Properties of Liquid Pyridine and Diazenes. *J. Mol. Struct.: THEOCHEM* **1998**, *424* (1−2), 145.
(49) McDonald, N. A.; Jorgensen, W. L. Development of an All-Atom Force Field for Heterocycles. Properties of Liquid Pyrrole, Furan, Diazoles, and Oxazoles. *J. Phys. Chem. B* **1998**, *102* (41), 8049.
(50) Rizzo, R. C.; Jorgensen, W. L. OPLS All-Atom Model for Amines: Resolution of the Amine Hydration Problem. *J. Am. Chem. Soc.* **1999**, *121* (20), 4827.
(51) Watkins, E. K.; Jorgensen, W. L. Perfluoroalkanes: Conformational Analysis and Liquid-State Properties from Ab Initio and Monte Carlo Calculations. *J. Phys. Chem. A* **2001**, *105* (16), 4118.
(52) Lee, F. L.; Barati Farimani, A.; Gu, K. L.; Yan, H.; Toney, M. F.; Bao, Z.; Pande, V. S. Solution-Phase Conformation and Dynamics of Conjugated Isoindigo-Based Donor-Acceptor Polymer Single Chains. *J. Phys. Chem. Lett.* **2017**, *8* (22), 5479.
(53) Sundaram, V.; Lyulin, A. v.; Baumeier, B. Development and Testing of an All-Atom Force Field for Diketopyrrolopyrrole Polymers with Conjugated Substituents. *J. Phys. Chem. B* **2020**, *124* (48), 11030.
(54) Kıbrıs, E.; Barbak, N. N.; Irmak, N. E. CHARMM Force Field Generation for a Cationic Thiophene Oligomer with FfTK. *J. Mol. Model.* **2021**, *27* (2), 34.
(55) Vanommeslaeghe, K.; Hatcher, E.; Acharya, C.; Kundu, S.; Zhong, S.; Shim, J.; Darian, E.; Guvench, O.; Lopes, P.; Vorobyov, I.; Mackerell, A. D. CHARMM General Force Field: A Force Field for Drug-like Molecules Compatible with the CHARMM All-Atom Additive Biological Force Fields. *J. Comput. Chem.* **2009**, *31*, 671.
(56) Michaels, W.; Zhao, Y.; Qin, J. Atomistic Modeling of PEDOT:PSS Complexes II: Force Field Parameterization. *Macromolecules* **2021**, *54* (12), 5354.
(57) Bhatta, R. S.; Yimer, Y. Y.; Tsige, M.; Perry, D. S. Conformations and Torsional Potentials of Poly(3-Hexylthiophene) Oligomers: Density Functional Calculations up to the Dodecamer. *Comput. Theor. Chem.* **2012**, *995*, 36.
(58) Higgins, J. S.; Benoit, H. C. *Polymers and Neutron Scattering*; Clarendon Press: New York, 1997.
(59) Lindner, P.; Zemb, T. *Neutrons, X-Rays and Light: Scattering Methods Applied to Soft Condensed Matter*; Elsevier Science: Amsterdam, 1988.
(60) Richter, D.; Monkenbusch, M.; Arbe, A.; Colmenero, J. *Neutron Spin Echo in Polymer Systems*; Springer, 2005.
(61) Arbe, A.; Alvarez, F.; Colmenero, J. Neutron Scattering and Molecular Dynamics Simulations: Synergetic Tools to Unravel Structure and Dynamics in Polymers. *Soft Matter* **2012**, *8* (32), 8257.
(62) Hammouda, B. *Probing Nanoscale Structures - The SANS Toolbox*; 2016.
(63) Zhan, P.; Zhang, W.; Jacobs, I. E.; Nisson, D. M.; Xie, R.; Weissen, A. R.; Colby, R. H.; Moulé, A. J.; Milner, S. T.; Maranas, J. K.; Gomez, E. D. Side Chain Length Affects Backbone Dynamics in Poly(3-alkylthiophene)s. *J. Polym. Sci., Part B: Polym. Phys.* **2018**, *56* (17), 1193.
(64) Wolf, C. M.; Guio, L.; Scheiwiller, S. C.; O'Hara, R. P.; Luscombe, C. K.; Pozzo, L. D. Blend Morphology in Polythiophene-Polystyrene Composites from Neutron and X-Ray Scattering. *Macromolecules* **2021**, *54* (6), 2960.
(65) Cao, Z.; Li, Z.; Zhang, S.; Galuska, L.; Li, T.; Do, C.; Xia, W.; Hong, K.; Gu, X. Decoupling Poly(3-Alkylthiophenes)' Backbone and Side-Chain Conformation by Selective Deuteration and Neutron Scattering. *Macromolecules* **2020**, *53* (24), 11142.
(66) Bastianini, F.; Pérez, G. E.; Hobson, A. R.; Rogers, S. E.; Parnell, A. J.; Grell, M.; Gutiérrez, A. F.; Dunbar, A. D. F. In-situ Monitoring Poly(3-Hexylthiophene) Nanowire Formation and Shape Evolution in Solution via Small Angle Neutron Scattering. *Sol. Energy Mater. Sol. Cells* **2019**, *202*, 110128.
(67) Guilbert, A. A. Y.; Zbiri, M.; Dunbar, A. D. F.; Nelson, J. Quantitative Analysis of the Molecular Dynamics of P3HT:PCBM Bulk Heterojunction. *J. Phys. Chem. B* **2017**, *121* (38), 9073.
(68) Pellegrini, E.; Calligari, P.; Calandrini, V.; Hinsen, K.; Kneller, G. R. *NMOLDYN User's Guide*, Version 3.4; 2009.
(69) Róg, T.; Murzyn, K.; Hinsen, K.; Kneller, G. R. *N* Moldyn: A Program Package for a Neutron Scattering Oriented Analysis of Molecular Dynamics Simulations. *J. Comput. Chem.* **2003**, *24* (5), 657.
(70) Brodeck, M.; Alvarez, F.; Arbe, A.; Juranyi, F.; Unruh, T.; Holderer, O.; Colmenero, J.; Richter, D. Study of the Dynamics of Poly(Ethylene Oxide) by Combining Molecular Dynamic Simulations and Neutron Scattering Experiments. *J. Chem. Phys.* **2009**, *130* (9), 094908.
(71) Pérez-Aparicio, R.; Arbe, A.; Alvarez, F.; Colmenero, J.; Willner, L. Quasielastic Neutron Scattering and Molecular Dynamics Simulation Study on the Structure Factor of Poly(Ethylene- *Alt* -Propylene). *Macromolecules* **2009**, *42* (21), 8271.


https://doi.org/10.1021/acspolymersau.1c00027
*ACS Polym. Au* 2021, 1, 134−152

(72) Tyagi, M.; Arbe, A.; Alvarez, F.; Colmenero, J.; González, M. A. Short-Range Order and Collective Dynamics of Poly(Vinyl Acetate): A Combined Study by Neutron Scattering and Molecular Dynamics Simulations. *J. Chem. Phys.* **2008**, *129* (22), 224903.
(73) Narros, A.; Arbe, A.; Alvarez, F.; Colmenero, J.; Zorn, R.; Schweika, W.; Richter, D. Partial Structure Factors in 1,4-Polybutadiene. A Combined Neutron Scattering and Molecular Dynamics Simulations Study. *Macromolecules* **2005**, *38* (23), 9847.
(74) Genix, A.-C.; Arbe, A.; Alvarez, F.; Colmenero, J.; Schweika, W.; Richter, D. Local Structure of Syndiotactic Poly(Methyl Methacrylate). A Combined Study by Neutron Diffraction with Polarization Analysis and Atomistic Molecular Dynamics Simulations. *Macromolecules* **2006**, *39* (11), 3947.
(75) Gerstl, C.; Brodeck, M.; Schneider, G. J.; Su, Y.; Allgaier, J.; Arbe, A.; Colmenero, J.; Richter, D. Short and Intermediate Range Order in Poly(Alkylene Oxide)s. A Neutron Diffraction and Molecular Dynamics Simulation Study. *Macromolecules* **2012**, *45* (17), 7293.
(76) Alvarez, F.; Colmenero, J.; Zorn, R.; Willner, L.; Richter, D. Partial Structure Factors of Polyisoprene: Neutron Scattering and Molecular Dynamics Simulation. *Macromolecules* **2003**, *36* (1), 238.
(77) Iradi, I.; Alvarez, F.; Colmenero, J.; Arbe, A. Structure Factors in Polystyrene: A Neutron Scattering and MD-Simulation Study. *Phys. B* **2004**, *350* (1−3), E881.
(78) Kneller, G. R.; Keiner, V.; Kneller, M.; Schiller, M. NMOLDYN: A Program Package for a Neutron Scattering Oriented Analysis of Molecular Dynamics Simulations. *Comput. Phys. Commun.* **1995**, *91* (1−3), 191.
(79) Hinsen, K.; Pellegrini, E.; Stachura, S.; Kneller, G. R. NMoldyn 3: Using Task Farming for a Parallel Spectroscopy-Oriented Analysis of Molecular Dynamics Simulations. *J. Comput. Chem.* **2012**, *33* (25), 2043.
(80) Walter, N. P.; Jaiswal, A.; Cai, Z.; Zhang, Y. LiquidLib: A Comprehensive Toolbox for Analyzing Classical and Ab Initio Molecular Dynamics Simulations of Liquids and Liquid-like Matter with Applications to Neutron Scattering Experiments. *Comput. Phys. Commun.* **2018**, *228*, 209.
(81) Manalastas-Cantos, K.; Konarev, P. v.; Hajizadeh, N. R.; Kikhney, A. G.; Petoukhov, M. v.; Molodenskiy, D. S.; Panjkovich, A.; Mertens, H. D. T.; Gruzinov, A.; Borges, C.; Jeffries, C. M.; Svergun, D. I.; Franke, D. *ATSAS 3.0*: Expanded Functionality and New Tools for Small-Angle Scattering Data Analysis. *J. Appl. Crystallogr.* **2021**, *54* (1), 343.
(82) Lindner, B.; Smith, J. C. Sassena - X-Ray and Neutron Scattering Calculated from Molecular Dynamics Trajectories Using Massively Parallel Computers. *Comput. Phys. Commun.* **2012**, *183* (7), 1491.
(83) Curtis, J. E.; Raghunandan, S.; Nanda, H.; Krueger, S. SASSIE: A Program to Study Intrinsically Disordered Biological Molecules and Macromolecular Ensembles Using Experimental Scattering Restraints. *Comput. Phys. Commun.* **2012**, *183* (2), 382.
(84) Arbe, A.; Alvarez, F.; Colmenero, J. Insight into the Structure and Dynamics of Polymers by Neutron Scattering Combined with Atomistic Molecular Dynamics Simulations. *Polymers* **2020**, *12* (12), 3067.
(85) Genix, A.-C.; Arbe, A.; Alvarez, F.; Colmenero, J.; Farago, B.; Wischnewski, A.; Richter, D. Self- and Collective Dynamics of Syndiotactic Poly(Methyl Methacrylate). A Combined Study by Quasielastic Neutron Scattering and Atomistic Molecular Dynamics Simulations. *Macromolecules* **2006**, *39* (18), 6260.
(86) Guilbert, A. A. Y.; Zbiri, M.; Finn, P. A.; Jenart, M.; Fouquet, P.; Cristiglio, V.; Frick, B.; Nelson, J.; Nielsen, C. B. Mapping Microstructural Dynamics up to the Nanosecond of the Conjugated Polymer P3HT in the Solid State. *Chem. Mater.* **2019**, *31* (23), 9635.
(87) Guilbert, A. A. Y.; Zbiri, M.; Jenart, M. V. C.; Nielsen, C. B.; Nelson, J. New Insights into the Molecular Dynamics of P3HT:PCBM Bulk Heterojunction: A Time-of-Flight Quasi-Elastic Neutron Scattering Study. *J. Phys. Chem. Lett.* **2016**, *7* (12), 2252.
(88) Guilbert, A. A. Y.; Urbina, A.; Abad, J.; Díaz-Paniagua, C.; Batallán, F.; Seydel, T.; Zbiri, M.; García-Sakai, V.; Nelson, J. Temperature-Dependent Dynamics of Polyalkylthiophene Conjugated Polymers: A Combined Neutron Scattering and Simulation Study. *Chem. Mater.* **2015**, *27* (22), 7652.
(89) Israelachvili, J. N. *Intermolecular and Surface Forces*, 3rd ed.; Elsevier Inc., 2011.
(90) Davies, P. L. Polarizabilities of Long Chain Conjugated Molecules. *Trans. Faraday Soc.* **1952**, *48*, 789.
(91) Schmit, J. D.; Levine, A. J. Statistical Model for Intermolecular Adhesion in Display = “inline“ $\pi$ -Conjugated Polymers. *Phys. Rev. Lett.* **2008**, *100* (19), 198303.
(92) Marchiori, C. F. N.; Koehler, M. Density Functional Theory Study of the Dipole across the P3HT:PCBM Complex: The Role of Polarization and Charge Transfer. *J. Phys. D: Appl. Phys.* **2014**, *47* (21), 215104.
(93) Price, A. J. A.; Bryenton, K. R.; Johnson, E. R. Requirements for an Accurate Dispersion-Corrected Density Functional. *J. Chem. Phys.* **2021**, *154* (23), 230902.
(94) Botu, V.; Batra, R.; Chapman, J.; Ramprasad, R. Machine Learning Force Fields: Construction, Validation, and Outlook. *J. Phys. Chem. C* **2017**, *121* (1), 511.
(95) Huan, T. D.; Batra, R.; Chapman, J.; Krishnan, S.; Chen, L.; Ramprasad, R. A Universal Strategy for the Creation of Machine Learning-Based Atomistic Force Fields. *npj Computational Materials* **2017**, *3* (1), 37.
(96) Jinnouchi, R.; Karsai, F.; Kresse, G. On-the-Fly Machine Learning Force Field Generation: Application to Melting Points. *Phys. Rev. B: Condens. Matter Mater. Phys.* **2019**, *100* (1), 014105.
(97) Unke, O. T.; Chmiela, S.; Sauceda, H. E.; Gastegger, M.; Poltavsky, I.; Schütt, K. T.; Tkatchenko, A.; Müller, K.-R. Machine Learning Force Fields. *Chem. Rev.* **2021**, *121* (16), 10142.
(98) Befort, B. J.; DeFever, R. S.; Tow, G. M.; Dowling, A. W.; Maginn, E. J. Machine Learning Directed Optimization of Classical Molecular Modeling Force Fields. *J. Chem. Inf. Model.* **2021**, *61* (9), 4400.
(99) Frenkel, D.; Smit, B. *Understanding Molecular Simulation: From Algorithms to Applications*, 2nd ed.; Academic Press: San Diego, 2001.


https://doi.org/10.1021/acspolymersau.1c00027
*ACS Polym. Au* 2021, 1, 134−152